

Diffraction of matter waves in space and in time

Časlav Brukner and Anton Zeilinger

Institut für Experimentalphysik, Universität Innsbruck, Technikerstrasse 25, A-6020 Innsbruck, Austria

(Received 26 December 1996)

In analogy to the well-known diffraction of waves at spatial structures, one can also define diffraction in time when a wave is temporarily modulated. In the present paper we investigate this phenomenon starting from a Green's-function approach. Diffraction in time appears for Schrödinger waves and not for light in vacuum. Specific cases of diffraction in time investigated here are diffraction at an "edge in time" and a Fresnel lens in time. We then investigate in detail the simultaneous diffraction both in space and in time representing a general solution. Then we analyze in detail diffraction at an edge, both in space and in time, of a single slit in space and in time, a double slit in space, and a single slit in time, a single slit in space and a double slit in time, and, finally, a double slit both in space and in time. In all cases we analyze the possibilities of various approximations which can be made, and show the limits and validity of the Fraunhofer approximation both in space and in time. We give explicit results for a gedanken experiment with very cold atoms. [S1050-2947(97)01909-4]

PACS number(s): 03.75.Be, 42.25.Fx, 42.50.Vk

I. INTRODUCTION

Diffraction in space implies a deviation from the geometrical path including deflection into the geometrical shadow. Analogously, diffraction in time implies that the wave can appear at the observation point at times different from the flight time of a classical particle. In the present paper we study phenomena appearing when both diffraction in space and in time happen together.

For a typical example of simultaneous diffraction in space and in time, consider a semi-infinite monochromatic wave, with wave vector \mathbf{k}_0 parallel to the x axis, which is blocked at $x=0$ by a nontransmitting screen containing a closed aperture and oriented perpendicular to the propagation direction. If at $t=0$ the aperture is opened, at time t what will be the probability density to observe the particle at the general position \mathbf{r} behind the slit?

It is well known that in the stationary case ($t \rightarrow \infty$ in the above example) both matter waves and electromagnetic waves show the same diffraction pattern. This is most directly seen by specifying a harmonic dependence on time $\psi(\mathbf{r}, t) = \phi(\mathbf{r})e^{-i\omega_0 t}$ as an ansatz for the Schrödinger equation in vacuum

$$\nabla^2 \psi(\mathbf{r}, t) + \frac{i2m}{\hbar} \frac{\partial \psi(\mathbf{r}, t)}{\partial t} = 0, \quad (1)$$

on the one hand, and for the wave equation in vacuum,

$$\nabla^2 \psi(\mathbf{r}, t) - \frac{1}{c^2} \frac{\partial^2 \psi(\mathbf{r}, t)}{\partial t^2} = 0, \quad (2)$$

on the other hand.¹ Then in both cases we obtain the same (Helmholtz) equation

$$\nabla^2 \phi(\mathbf{r}) + k_0^2 \phi(\mathbf{r}) = 0 \quad (3)$$

for the stationary solution. The wave number k_0 is $\sqrt{2m\omega_0/\hbar^2}$ for the Schrödinger equation and ω_0/c for the wave equation.

Inspecting the symmetry between space and time coordinates in the wave equation (that is, the fact that the derivatives of both space and time coordinates are of second order), and knowing that electromagnetic waves exhibit diffraction in space in the nonstationary case, one might be tempted naïvely to assume that diffraction in time occurs for electromagnetic waves. However, diffraction in time does not occur for the wave equation [3], but, in contrast, arises for the Schrödinger equation [3–7]. Moreover, despite the fact that the Schrödinger equation is of parabolic type, while the Helmholtz equation is elliptic, there is a close resemblance between the matter wave diffraction patterns in time and the stationary diffraction patterns in space.

The problem of nonstationary diffraction effects of matter waves appears to have first been discussed by Moshinsky [3]. Involving certain initial conditions in space, he considered the problem of wave evolution following the instantaneous removal of an ideal nontransmitter from a semi-infinite monochromatic beam. He found a solution closely

¹Evidently, electromagnetic waves are vector waves. Yet it can be shown that in free space [1] and in some cases even inside media [2], one can use the scalar wave equation. In general, it takes quite a calculation and specific assumptions to derive this result. It was shown in Ref. [1] that, for example, the intensity of natural light in vacuum can be represented in terms of a single complex scalar wave function if the electrical and magnetic fields do not vary appreciably over the wave front.

related to the stationary one for diffraction of a plane wave at an edge in space.

The dispersion relations lie at the heart of diffraction in time phenomena. The relation between frequency and wave vector as given by the Schrödinger equation is $\omega(\mathbf{k}) = |\mathbf{k}|^2 \hbar / 2m$. Thus an initial wave with group velocity \mathbf{v}_0 and with a sharp wave front at some instant will instantaneously spread over all space. Actually, in order to obtain a sharp front, one requires infinitely large momentum components, which for Schrödinger waves would imply infinite (signal) velocities and instantaneous spreading. Consequently, an observer at distance $|\mathbf{r}|$ could detect a particle before the flight time $|\mathbf{r}|/|\mathbf{v}_0|$ of a classical particle. In the case of an electromagnetic wave such a dispersion would imply detection of the particles before the time $|\mathbf{r}|/c$. Conversely, since the wave equation involves only derivatives of the same (second) order in space and in time, there is no dispersion, and the wave front of the initial wave packet propagates with the limiting velocity c . Therefore, there is no diffraction in time for light. For completeness we mention here that, in general, for electromagnetic waves, and thus for photons, diffraction in time can indeed occur in a medium. This is because, inside a medium, we find dispersion relations which significantly deviate from the linear free-space behavior.

The above-mentioned symmetry of space and time coordinates in the wave equation is sufficient for equivalence between phenomena in space and in time only in one-dimensional problems, while the observation of diffraction in space requires at least two dimensions. A wave emitted by a point source (Green's function) obeying the wave equation in vacuum will be concentrated at time t on a sphere of radius ct whose center is at the source point. The wave function represented by the superposition of the effects of many point sources in an aperture can thus also differ from zero in regions inside the geometric shadow, but only after time L/c (L is the distance to the nearest point in the aperture). Thus light propagating in vacuum exhibits diffraction in space but not in time.

In contrast, the Green's function of the nonrelativistic Schrödinger equation immediately becomes unequal zero everywhere as soon as t differs from zero because a point source δ disturbance contains all velocity components. Therefore at some fixed space point the wave function builds up continuously from $t=0$. Thus matter waves diffract both in space and in time.²

In Sec. II the Green's-function approach to solving linear, partial, and in general inhomogeneous differential equations with inhomogeneous boundary conditions is applied to the Schrödinger equation modified to contain a source term. Using superposition, both the source term and the inhomogeneous boundary condition are treated as collections of coherent point sources.

²A wave originating at a point source and obeying the Schrödinger equation can be expressed as a product of the individual waves propagating in independent (x , y , and z) directions. This implies that after passing an aperture the deflection of a matter wave into the geometric shadow is due to the independent dispersions along these directions, rather than being a consequence of correlated propagation along different directions contained in the nonseparability of the electromagnetic Green's function.

Involving boundary conditions to solve nonstationary problems, in the present paper we introduce conditions in time analogous to the boundary conditions in space used in stationary spatial diffraction. Hence, in Sec. III A we use an "edge in time" boundary condition to solve Moshinsky's problem. In order to extend the analogy between stationary optics in general and nonstationary optics of matter waves further, in Sec. III B we introduce Fresnel zones in time, and illustrate this by introducing a Fresnel lens in time. In Sec. IV, combining the conditions in space with the conditions in time, we compute different two-dimensional problems which permit us to discuss simultaneous diffraction and interference effects in space and in time. The solutions obtained hold when the conditions for strong diffraction effects in space and in time are satisfied, i.e., when the wavelength and the wave period of the de Broglie wave are of the same order as the slit width and the slit opening time, respectively. We also identify that parameter regime where the space and time dependences of the diffraction patterns are equivalent.

It is a challenging research program to exhibit diffraction and interference effects for increasingly larger objects. We emphasize therefore that the physical parameters considered in Sec. IV for the experimental realization of phenomena discussed in the present paper may be accessible with cold atoms. It is well known in the theory of stationary diffraction that the diffraction pattern in the Fraunhofer limit represents the square of the Fourier transform in space of the incident wave in the aperture. In Sec. V we examine under which conditions one can generalize such considerations to the nonstationary diffraction patterns in space and in time. Finally Sec. VI is reserved for some concluding remarks.

II. POINT SOURCES OF MATTER WAVES IN SPACE AND IN TIME

In this section we first determine the solution of the time-dependent Schrödinger equation in vacuum modified to contain a source term. Using superposition, both the source term of the differential equation and the inhomogeneous boundary condition can be treated as collections of mutually coherent point sources. This yields an exact solution in the form of an integral.

The Schrödinger equation in vacuum (1) modified to contain the inhomogeneous source term $\rho(\mathbf{r}, t)$,

$$\nabla^2 \psi(\mathbf{r}, t) + \frac{i2m}{\hbar} \frac{\partial \psi(\mathbf{r}, t)}{\partial t} = -4\pi\rho(\mathbf{r}, t), \quad (4)$$

is an example of a linear, partial, and inhomogeneous differential equation. Although the source density $\rho(\mathbf{r}, t)$ has no immediate physical meaning, we introduce it for mathematical completeness. This will facilitate the treatment of certain boundary conditions and initial conditions. For each type of equation there is a definite set of initial conditions and boundary conditions which will give unique solutions, and any other conditions will give either nonunique or impossible answers. The boundary conditions may be given in different types. The specification on the boundary surface of the value $\psi(\mathbf{r}, t)$ is called the Dirichlet condition. The Neumann condition is given when the normal derivative of the function $\psi(\mathbf{r}, t)$ on the boundary is defined. When a linear combina-

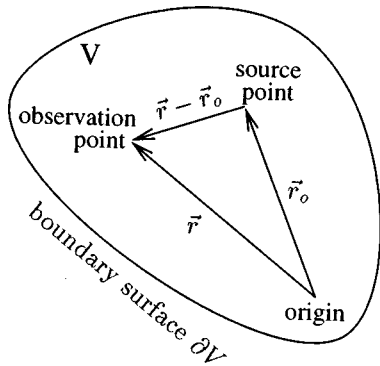


FIG. 1. Source point \mathbf{r}_0 , observation point \mathbf{r} , boundary surface ∂V , and volume V considered in the text.

tion of the function $\psi(\mathbf{r}, t)$ and its normal derivative are given on the boundary, it is called a mixed boundary condition. Depending on whether the values of the boundary data vanish or not, we speak about homogeneous or inhomogeneous boundary conditions, respectively. The condition on the boundary surface for the Schrödinger equation may be either Dirichlet or Neumann or mixed [8].

The linearity of the differential equation (4) has the consequence that the sum of the solutions for different individual sources is a solution of the equation with the sum of the sources present. With the point source solution, one can thus obtain the solution for an arbitrary source distribution. The solution of the equation

$$\begin{aligned} \nabla^2 G(\mathbf{r}, t, \mathbf{r}_0, t_0) + \frac{i2m}{\hbar} \frac{\partial G(\mathbf{r}, t, \mathbf{r}_0, t_0)}{\partial t} \\ = -4\pi \delta^3(\mathbf{r} - \mathbf{r}_0) \delta(t - t_0) \end{aligned} \quad (5)$$

is called the Green's function for the Schrödinger equation in vacuum. Generally, the Green's function $G(\mathbf{r}, t, \mathbf{r}_0, t_0)$ can be understood to describe, within the volume V enclosed by the surface ∂V (Fig. 1), the effect on the observation point \mathbf{r} at time t of a point source localized at position \mathbf{r}_0 at time t_0 .

Morse and Feshbach [8] gave integral forms of solutions for several linear partial equations. Inserting the imaginary square $a^2 = -i(2m/\hbar)$ of the diffusion constant a into the results (p. 857 in Ref. [8]) for the diffusion equation: $\nabla^2 \psi(\mathbf{r}, t) = a^2 [\partial \psi(\mathbf{r}, t) / \partial t]$, one may immediately obtain the corresponding expressions for the Schrödinger equation. In the following we briefly discuss these expressions.

To ensure the existence and uniqueness of the Green's function, we let it obey certain boundary conditions and initial conditions. It is sufficient to consider that Green's function which satisfies the homogeneous form of the boundary condition with respect to the variable \mathbf{r} , either Dirichlet,

$$G(\mathbf{r}, t, \mathbf{r}_0, t_0) = 0, \quad \mathbf{r} \in \partial V,$$

or Neumann,

$$\nabla G(\mathbf{r}, t, \mathbf{r}_0, t_0) = \mathbf{0}, \quad \mathbf{r} \in \partial V, \quad (6)$$

or mixed. Physical reasoning forces initial conditions on the Green's function. The disturbance at point \mathbf{r}_0 at time t_0 has an influence on other space points only at later times $t > t_0$

(causality).³ Thus

$$G(\mathbf{r}, t, \mathbf{r}_0, t_0) = 0 \quad \text{and} \quad \nabla G(\mathbf{r}, t, \mathbf{r}_0, t_0) = \mathbf{0} \quad \text{for } t < t_0. \quad (7)$$

Using the boundary conditions (6) and causality (7), the solution of the modified Schrödinger equation (4) can be represented in integral form [8]:

$$\begin{aligned} \psi(\mathbf{r}, t) = \int_0^{t^+} dt_0 \int_V dV_0 \rho(\mathbf{r}_0, t_0) G(\mathbf{r}, t, \mathbf{r}_0, t_0) \\ + \frac{im}{2\pi\hbar} \int_V dV_0 G(\mathbf{r}, t, \mathbf{r}_0, 0) \psi(\mathbf{r}_0, 0) \\ + \frac{1}{4\pi} \int_0^{t^+} dt_0 \int_{\partial V} d\mathbf{S}_0 [G(\mathbf{r}, t, \mathbf{r}_0, t_0) \nabla_0 \psi(\mathbf{r}_0, t_0) \\ - \psi(\mathbf{r}_0, t_0) \nabla_0 G(\mathbf{r}, t, \mathbf{r}_0, t_0)]. \end{aligned} \quad (8)$$

The vector $d\mathbf{S}_0$ represents an element of the boundary surface ∂V and points outward, away from the volume V inside the boundary. The first integral in Eq. (8) represents the effects of volume sources, the second one the effects of the initial condition, while the last one includes the effects of the boundary condition.

Contrary to the Schrödinger equation, the initial conditions for the wave equation are of the Cauchy type. This means that uniqueness of the solution requires at every space point considered not only the specification of the initial wave function, but also of its initial derivative in time. This is a consequence of the second derivative in time in the wave equation (2). The boundary conditions are of the same type for both the Schrödinger and the wave equation. Thus the integral representation of the solution of the wave equation appears in the form [8]

$$\begin{aligned} \psi^{\text{light}}(\mathbf{r}, t) = \int_0^{t^+} dt_0 \int_V dV_0 \rho(\mathbf{r}_0, t_0) G(\mathbf{r}, t, \mathbf{r}_0, t_0) \\ - \frac{1}{c^2} \int_V dV_0 \left[\frac{\partial G(\mathbf{r}, t, \mathbf{r}_0, t_0)}{\partial t_0} \Big|_{t_0=0} \psi(\mathbf{r}_0, 0) \right. \\ \left. - G(\mathbf{r}, t, \mathbf{r}_0, 0) \frac{\partial \psi(\mathbf{r}_0, t_0)}{\partial t_0} \Big|_{t_0=0} \right] \\ + \frac{1}{4\pi} \int_0^{t^+} dt_0 \int_{\partial V} d\mathbf{S}_0 [G(\mathbf{r}, t, \mathbf{r}_0, t_0) \nabla_0 \psi(\mathbf{r}_0, t_0) \\ - \psi(\mathbf{r}_0, t_0) \nabla_0 G(\mathbf{r}, t, \mathbf{r}_0, t_0)]. \end{aligned}$$

³For the case of waves which do not have a wave front and a limiting (signal) velocity (which is the case for Schrödinger waves) the Schuetzer-Tiomno causality condition [9] is to be applied. It reads as follows: the scattered wave packet at a distance $|\mathbf{r}|$ at time t cannot depend on the behavior of the incoming wave packet at $|\mathbf{r}'|$ at later times $t > t_0$, i.e., $G(\mathbf{r}, t, \mathbf{r}_0, t_0) = 0$ for $t < t_0$. The condition used by us is a stronger condition.

Employing the Green's function, one can obtain a solution of the inhomogeneous equation with the given homogeneous boundary condition, or else the solution of the homogeneous equation with an inhomogeneous boundary condition. Because of the linearity of the equation it is also possible to solve the inhomogeneous equation with an inhomogeneous boundary condition by superposition of both types of solutions. It might not be clear how the Green's function, as a solution of the *inhomogeneous* equation (5) satisfying the *homogeneous* boundary condition, could help us to solve a *homogeneous* equation with an *inhomogeneous* boundary condition. In order to make this more understandable, we can apply a well-known recipe used in electrostatic problems. Replacing the inhomogeneous condition on the boundary surface by a homogeneous one together with an appropriate surface distribution of sources (a double layer for Dirichlet conditions and a single layer for Neumann conditions) just inside the surface, one reduces the case of the homogeneous equation with inhomogeneous boundary condition to the case of the inhomogeneous equation with homogeneous boundary condition.

Pointing again to Ref. [8], where the exact and detailed evolution is treated, here we briefly analyze the Green's function for the Schrödinger equation in vacuum for an infinite volume (i.e., for a free particle)

$$G_0(|\mathbf{r}-\mathbf{r}_0|, t-t_0) = \left(\frac{m}{2\pi i\hbar}\right)^{1/2} \frac{1}{(t-t_0)^{3/2}} e^{im|\mathbf{r}-\mathbf{r}_0|^2/2\hbar(t-t_0)} \theta[t-t_0], \quad (9)$$

where $\theta[t-t_0] \equiv 1$ for $t \geq t_0$, and 0 for $t < t_0$, is the step function required by causality. Since we are dealing with a point source in an infinite homogeneous and isotropic volume, G_0 is rather a function of $|\mathbf{r}-\mathbf{r}_0|$ than of \mathbf{r} and \mathbf{r}_0 separately. As soon as $t-t_0$ differs from zero, the Green's function immediately becomes nonzero everywhere. This shows that we are dealing with nonrelativistic quantum mechanics.

A particle propagating from position \mathbf{r}_0 at time t_0 to the point \mathbf{r} at time t moves with the velocity $\mathbf{V} = (\mathbf{r}-\mathbf{r}_0)/(t-t_0)$. Using this expression in the definition of the wave vector $\mathbf{K} \equiv m\mathbf{V}/\hbar$ and the frequency $\Omega \equiv m\mathbf{V}^2/2\hbar$ of the de Broglie wave, the corresponding phase $\mathbf{K}(\mathbf{r}-\mathbf{r}_0) - \Omega(t-t_0) = m|\mathbf{r}-\mathbf{r}_0|^2/2\hbar(t-t_0)$ matches exactly that of the Green's function (9). Considering every Green's function as a representation of a unitary evolution operator $G(\mathbf{r}, t, \mathbf{r}_0, t_0) \equiv \langle \mathbf{r} | \hat{U}(t, t_0) | \mathbf{r}_0 \rangle$ and inserting $G_0(|\mathbf{r}-\mathbf{r}_0|, t-t_0) = c(t-t_0) e^{im|\mathbf{r}-\mathbf{r}_0|^2/2\hbar(t-t_0)} \theta[t-t_0]$ into the unitarity condition $\hat{U}(t, t_0) \hat{U}^\dagger(t, t_0) = \hat{I}$, the norm $|c(t-t_0)|$ will be fixed leading, besides a phase factor, to Eq. (9). Since a conservative system (free evolution) is considered, the time dependence of the unitary operator appears in the form $t-t_0$.

The Green's function for the wave equation in vacuum (2) is a spherical shell around the point source, expanding with the radial velocity c [8],

$$G_0^{\text{light}}(|\mathbf{r}-\mathbf{r}_0|, t-t_0) = \frac{\delta[|\mathbf{r}-\mathbf{r}_0|/c - (t-t_0)]}{|\mathbf{r}-\mathbf{r}_0|} \theta[t-t_0].$$

III. DIFFRACTION IN TIME

The problem of the evolution of a matter wave incident on a time-dependent aperture has been treated theoretically by several authors [3–7]. In the simplest case it is a one-dimensional problem. The first step toward its solution was made by Moshinsky [3], who analyzed the wave evolution following the instantaneous removal of an ideal nontransmitting screen from a semi-infinite monochromatic beam $\psi(x, 0) = e^{ik_0x} \theta[-x]$. Involving this initial condition and the Green's function for a free particle (9), he performed calculations of the last volume integral in Eq. (8). Yet the initial condition approach is difficult to realize in the general case of a screen containing a time-dependent aperture. This is because the Green's functions of such two- or three-dimensional problems are very difficult to calculate for an infinite volume, and to our knowledge have not yet been obtained, not even for the simplest aperture opening functions. On the other hand, if we restrict our considerations to the positive half-space (at the right of the screen), we can solve the problem by computing the surface integral in Eq. (8) with appropriate boundary conditions in the plane of the screen and with the corresponding Green's function always satisfying the differential equation (5) in the volume considered. Then the exact form of the Green's function depends only on the specific type of boundary condition.

The second reason for using the boundary condition approach is to complete the analogy between diffraction in time and stationary diffraction in space. The integration over time, contained in the integral involving boundary conditions, makes it possible to introduce conditions in time analogous to the conditions over space in stationary spatial diffraction. Hence a sudden removal and replacement of the screen is represented by an appropriate range of integration over time (in the one-dimensional problem the integral expressing the effects of the boundary conditions reduces to one over time only). This is a time analog of a slit in a screen in stationary diffraction, represented by a corresponding integration over spatial coordinates at the boundary surface. We now turn to a more detailed discussion of Moshinsky's problem, intending to solve it using the boundary condition approach.

A. Edge in time

We consider a semi-infinite plane matter wave propagating parallel to the x axis from left to right, being stopped by a nontransmitting screen placed at $x=0$ oriented perpendicular to the propagation direction. All of a sudden the screen is removed at $t=0$, marking the beginning of propagation of particles along the positive- x axis. In order to calculate the time evolution of the probability of finding the particle at points $x>0$ for times $t>0$, we assume the Dirichlet boundary condition $\psi(0, t) = e^{-i\omega_0 t} \theta[t]$ at the plane $x=0$. We expect that the semi-infinite monochromatic time dependence of the boundary condition is close to the actual time dependence at $x=0$ caused by the free propagation of a semi-infinite plane wave. However, a difference will arise at the end of the calculation, and will be discussed there. Additionally we assume⁴ that for every finite time t of observation the solution tends to zero for $x \rightarrow \infty$.

The corresponding Green's function, satisfying the homogeneous Dirichlet condition at the boundary plane $x=0$, can

be constructed as in electrostatics with the image method. There an image point source to the left of the boundary is assigned to each point source to the right. The contributions of both sources are then superposed to satisfy the given homogeneous boundary condition. In the case of the homogeneous Dirichlet condition the real point source and its image have opposite signs:

$$G(\mathbf{r}, t, \mathbf{r}_0, t_0) = G_0(|\mathbf{r} - \mathbf{r}_0|, t - t_0) - G_0(|x + x_0|, |y - y_0|, |z - z_0|, t - t_0), \quad (10)$$

where $G_0(|\mathbf{r} - \mathbf{r}_0|, t - t_0)$ is the free propagator (9). The Green's function (10) is still the solution of the differential equation (5) because the image source lies outside of the half-space considered. Since the Green's function (10) is zero at the plane $x_0 = 0$, the first term in the surface integral in Eq. (8) vanishes, leaving

$$\psi(x, t) = -\frac{1}{4\pi} \int_0^{t+} dt_0 \int_{x_0=0} d\mathbf{S}_0 \psi(\mathbf{r}_0, t_0) \nabla_0 G(\mathbf{r}, t, \mathbf{r}_0, t_0). \quad (11)$$

After integration over y and z , we obtain

$$\begin{aligned} \psi(x, t) &= x \left(\frac{m}{2\pi\hbar} \right)^{1/2} e^{-i(\pi/4)} \\ &\times \int_0^t dt_0 \frac{1}{(t-t_0)^{3/2}} \\ &\times e^{-i\omega_0 t_0} e^{imx^2/2\hbar(t-t_0)}. \end{aligned} \quad (12)$$

Changing the integration variable to $\xi = 1/\sqrt{t-t_0}$, we find

$$\begin{aligned} \psi(x, t) &= \frac{x}{2} \left(\frac{m}{2\pi\hbar} \right)^{1/2} e^{-i(\pi/4)} e^{-i\omega_0 t} \\ &\times \int_{1/\sqrt{t}}^{\infty} d\xi e^{i\omega_0/\xi^2} e^{(imx^2/2\hbar)\xi^2}. \end{aligned}$$

We evaluate this integral using the solution

⁴In the corresponding time-dependent electromagnetic problem one can always find a distance larger than ct (t is the observation time) such that both $\psi(\mathbf{r}, t)$ and $\partial\psi(\mathbf{r}, t)/\partial\mathbf{r}$ are zero. Since the waves obeying the Schrödinger equation spread with infinite velocity, our assumption is not trivial. Here we content ourselves with the plausible argument that the distance \mathbf{r} can always be chosen larger by any order than vt (v is the classical velocity of a particle), such that the norms of both $\psi(\mathbf{r}, t)$ and $\partial\psi(\mathbf{r}, t)/\partial\mathbf{r}$ can be arbitrarily close to zero.

$$\begin{aligned} \int d\xi e^{-a^2\xi^2} e^{-b^2/\xi^2} &= \frac{\sqrt{\pi}}{4a} \left(e^{2ab} \operatorname{erf} \left[a\xi + \frac{b}{\xi} \right] \right. \\ &\left. + e^{-2ab} \operatorname{erf} \left[a\xi - \frac{b}{\xi} \right] \right) + \text{const}, \end{aligned} \quad (13)$$

from the integral tables [10] with $-a^2 = i\omega_0$ and $-b^2 = imx^2/2\hbar$. Transforming the error functions into the Fresnel integrals $F[z] \equiv \int_0^z du e^{i(\pi/2)u^2} \in \mathbb{C}$, $z \in \mathbb{R}$, $\operatorname{erf}[z/\sqrt{i}] = \sqrt{2/i} F[z\sqrt{2/\pi}]$, one finally obtains

$$\begin{aligned} \psi(x, t) &= \frac{1}{\sqrt{2}} e^{-i(\pi/4)} e^{-i\omega_0 t} \left\{ e^{ik_0 x} \left(F \left[\frac{2}{\sqrt{Tt}} (t - \tau_{cl}) \right] \right. \right. \\ &\quad \left. \left. - F[-\infty] \right) + e^{-ik_0 x} \left(F \left[-\frac{2}{\sqrt{Tt}} (t + \tau_{cl}) \right] \right. \right. \\ &\quad \left. \left. - F[-\infty] \right) \right\}, \end{aligned} \quad (14)$$

where $k_0 \equiv \sqrt{2m\omega_0/\hbar}$ and $T \equiv 2\pi/\omega_0$ are the wave number and the wave period of the de Broglie wave, respectively, and $\tau_{cl} \equiv mx/k_0\hbar$ is the time a classical particle needs to travel from 0 to x . The first term in Eq. (14) is Moshinsky's solution [3] [see Eq. (15) below], freely evolving from the initial wave $e^{ik_0 x} \theta[-x]$. It can be shown that the second term is freely evolving from the initial wave $e^{-ik_0 x} \theta[-x]$. Therefore, if we restrict our considerations to the right half-space, the wave evolved under the boundary condition $e^{-i\omega_0 t} \theta[-t]$ at $x=0$ is equivalent to the freely evolving initial wave $(e^{ik_0 x} + e^{-ik_0 x}) \theta[-x]$.

It is expected that the contribution of the initial wave propagating to the left is negligible in the right half-space. Actually, fixing the space point x , the argument of the third Fresnel integral in Eq. (14) has its maximum value of $-4\sqrt{\tau_{cl}/T}$ at $t = \tau_{cl}$. This maximum tends to negative infinity for $\lambda \ll x$, i.e., $T \ll \tau_{cl}$ ($\lambda \equiv 2\pi/k_0$ is the de Broglie wavelength), leaving only Moshinsky's solution

$$\begin{aligned} \psi^{\text{Mosh.}}(x, t) &= \frac{1}{\sqrt{2}} e^{-i(\pi/4)} e^{i(k_0 x - \omega_0 t)} \\ &\times \left(F \left[\frac{2}{\sqrt{Tt}} (t - \tau_{cl}) \right] - F[-\infty] \right). \end{aligned} \quad (15)$$

At this point we shall review some properties of Moshinsky's solution. Moshinsky's solution has a remarkable analytical similarity to the solution $(1/\sqrt{2})e^{-i(\pi/4)}e^{i(k_0 x - \omega_0 t)}(F[\sqrt{2/\lambda xy}] - F[-\infty])$ for stationary diffraction of a plane wave at an edge. The classically expected cutoff at $x = \hbar k_0 t/m$ is smeared out because the initial wave consists of different momentum components propagating with different velocities. The intensity given by Moshinsky's solution (Fig. 2) differs appreciably from zero only when t is of the order of or larger than the time of flight τ_{cl} of the classical particle. At the time $t = \tau_{cl}$ the intensity is exactly 25% of the incident intensity. The analogous point in stationary diffraction of a plane wave at an edge is the position of the edge projected onto the observation screen. There

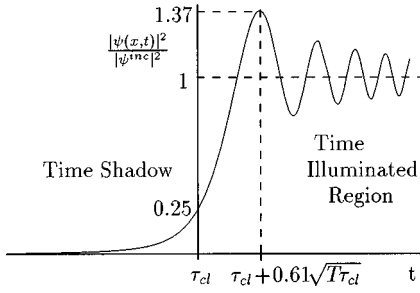


FIG. 2. Intensity at a fixed-space point as a function of time for the case of diffraction at an edge in time of an incident matter wave with wave period T . At the classical time $t = \tau_{cl}$ and at the first maximum in time $t = \tau_{cl} + 0.61\sqrt{T\tau_{cl}}$ for $T \ll \tau_{cl}$, the intensity is exactly 25% and 137%, respectively, of the incident intensity, the latter being equivalent to the intensity when $t \rightarrow \infty$. The transitional time from “time shadow” to “time illuminated region” is of the order of $\sqrt{T\tau_{cl}}$ for $T \ll \tau_{cl}$.

too the intensity is 25% of the intensity level with no edge present. The transitional time from the “time shadow” ($t < \tau_{cl}$) to the “time-illuminated region” ($t > \tau_{cl}$) is of the order of $\sqrt{T\tau_{cl}}$ for $T \ll \tau_{cl}$. More precisely, for $T \ll \tau_{cl}$ the intensity reaches its maximal value of 137% of the incident intensity at $t = \tau_{cl} + 0.61\sqrt{T\tau_{cl}}$. Analogously, in stationary diffraction at an edge, the range over which the shadow is not sharp is of the order of $\sqrt{\lambda x}$. With further increasing time the intensity oscillates in a damped fashion around the incident intensity, the latter being equivalent to the intensity of Moshinsky’s solution when $t \rightarrow \infty$. Similarly, going from the light-shadow boundary into the illuminated region, the intensity for the stationary diffraction of a plane wave at an edge oscillates in a damped fashion around the incident intensity.

Therefore, for $T \ll \tau_{cl}$, there is a close relationship between the solution for the diffraction at an edge in time and the one for stationary diffraction at an edge in space. The condition of a step function screen opening and the close mathematical resemblance with the stationary solution of diffraction at the edge are the reasons for calling the present case an “edge in time.” The difference between diffraction at the edge in time and stationary edge diffraction is that the nonstationary solution vanishes for $t < 0$, while the solution of the stationary problem differs from zero for all values of the y coordinate. This difference emerges due to well-defined starting time of the inhomogeneous boundary condition.

We also want to emphasize a close resemblance between the solution for light diffraction at the edge in time and the solution for matter wave diffraction at the edge in time in the classical limit. Expressing solutions (14) through the classical velocity v_0 instead of k_0 and ω_0 , and letting Planck’s constant h tend to zero and/or the mass m tend to infinity, the time transitional period tends to zero and the solution reduces to the classical one:

$$\lim_{h \rightarrow 0} \psi_{\text{mat}}(\mathbf{r}, t) = e^{ik_0(x - v_0 t)} \theta[v_0 t - x].$$

Dealing with the same problem for electromagnetic waves instead of matter waves, we obtain the solution

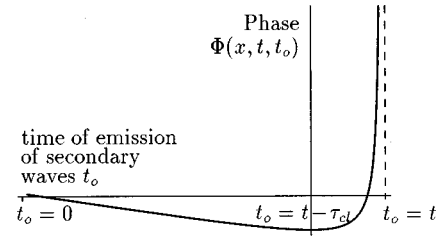


FIG. 3. Dependence of the phase of the secondary wave on the time of its emission $t_0 \in [0, t]$ at a fixed-space point x at the fixed time t . The secondary wave is emitted from the $x = 0$ plane, where the boundary condition $e^{-i\omega_0 t} \theta[t]$ is defined. The phase is stationary at the time $t_0 = t - \tau_{cl}$ ($\tau_{cl} \equiv \sqrt{mx^2/2\hbar\omega_0}$ is the flight time of the classical particle), when the classical particle moving with the classical velocity τ_d would be emitted.

$$\psi_{\text{light}}(\mathbf{r}, t) = e^{ik_0(x - ct)} \theta[ct - x]$$

which also exhibits no diffraction in time effects. A similar solution was found by Moshinsky [3] using the initial condition approach.

B. Fresnel zones in time

Huygens’s principle postulating that each point on the wave front acts as a point source of secondary waves supplemented by Fresnel with the statement that these secondary waves are mutually coherent and interfere, is basic for the Fresnel zone method of an intuitive description of stationary diffraction. Thus dividing the front of an incident plane wave into annular zones in such a way that the distances between zone boundaries and the observation point vary in steps of $\lambda/2$, and letting the secondary waves arriving from different zones interfere, we can determine the amplitude at the observation point for any number of open zones.

The solution involving time-dependent boundary conditions is equivalent to one for an appropriate time-dependent distribution of sources over the boundary surface, thus extending Huygens’ and Fresnel’s principles to nonstationary problems. Then $\psi(\mathbf{r}, t)$ satisfying the inhomogeneous Dirichlet condition may be interpreted as a superposition of secondary waves emitted from a double layer of a magnitude of “dipole” moment density proportional to the value $\psi(\mathbf{r}, t)$ at the boundary [8].

Here we are interested in the solution in the right half-space when the Dirichlet condition $e^{-i\omega_0 t_0} \theta[t_0]$ at the boundary surface $x = 0$ is defined. We shall now calculate a secondary wave $\psi^{s.\text{wave}}(x, t, t_0)$ emitted at t_0 from a double layer with dipole moment density of uniform magnitude proportional to $e^{-i\omega_0 t_0}$. From Eq. (11), we obtain

$$\begin{aligned} \psi^{s.\text{wave}}(x, t, t_0) &= \frac{1}{4\pi} \int_{-\infty}^{\infty} dy_0 \int_{-\infty}^{\infty} dz_0 e^{-i\omega_0 t_0} \left. \frac{\partial G(\mathbf{r}, t, \mathbf{r}_0, t_0)}{\partial x_0} \right|_{x_0=0} \\ &= x \left(\frac{m}{2\pi i \hbar} \right)^{1/2} \frac{1}{(t - t_0)^{3/2}} e^{-i\omega_0 t_0} e^{imx^2/2\hbar(t - t_0)}. \end{aligned} \quad (16)$$

Thus the phase of the secondary wave emitted at t_0 is at point x at time t (Fig. 3)

$$\phi(x, t, t_0) = -\omega_0 t_0 + \frac{mx^2}{2\hbar(t-t_0)}. \quad (17)$$

Notice that this is just the phase of the integrand in Eq. (12).

Now we will divide the time axis t_0 into zones in such a way that the phases of the secondary waves emitted at the zone boundaries differ by π when arriving at the fixed point x at time t . Denoting the boundaries of the zones in time by $t_0^0, t_0^{\pm 1}, \dots, t_0^{\pm n}, \dots, n \in \mathbb{N}$, we can write this condition in the form

$$\begin{aligned} \phi(x, t, t_0^{\pm 1}) - \phi(x, t, t_0^0) &= \pi, \\ \phi(x, t, t_0^{\pm 2}) - \phi(x, t, t_0^{\pm 1}) &= \pi, \\ &\dots, \\ \phi(x, t, t_0^{\pm n}) - \phi(x, t, t_0^{\pm n-1}) &= \pi \\ &\dots, \end{aligned} \quad (18)$$

Realizing that the phase (17) is stationary for a classical particle moving with the velocity $\sqrt{2\hbar\omega_0/m}$ and arriving at point x at time t (see Fig. 3), the center of the zeroth zone is defined by $t-t_0^0 = \tau_{cl}$, where $\tau_{cl} \equiv \sqrt{mx^2/2\hbar\omega_0}$ is the flight time of a classical particle. Consequently, the zone boundaries are given by

$$t_0^{\pm n} = t - \tau_{cl} - \frac{nT}{4} \pm \left[\left(\tau_{cl} + \frac{nT}{4} \right)^2 - \tau_{cl}^2 \right]^{1/2}. \quad (19)$$

When $T \ll \tau_{cl}$, we obtain, with an error not exceeding nT ,

$$t_0^{\pm n} = t - \tau_{cl} \pm \left(\frac{nT\tau_{cl}}{2} \right)^{1/2}.$$

In the stationary case of propagation of a plane wave, the distance between the zeroth and n th Fresnel annular zone is, up to a term of the order of $n\lambda$, analogously given by $\sqrt{xn\lambda}$, $n \in \mathbb{Z}$, where x is the distance between the observation point and the plane of sources of secondary waves. This shows the fact that close to the zeroth zones the arrangements of the Fresnel zones in time and of the stationary Fresnel zones in space are equivalent.

As in stationary optics, we now proceed by dividing each zone into a number of m subzones such that the phase change from one subzone to the next is of the order of π/m . As we move away from the zeroth zone the lengths of the Fresnel zones decrease [Fig. 4(a)], and consequently the amplitude of the wave arriving from each subzone decreases. Additionally taking into account that the amplitude of the secondary wave $\psi^{s.wave}(x, t, t_0)$ is proportional to $1/(t-t_0)^{3/2}$ [see Eq. (16)], graphic addition of the amplitudes in the complex plane leads to a spiral as shown in Fig. 4(b), analogous to the Cornu spiral for stationary diffraction. We recall that the radius of curvature of the Cornu spiral for stationary diffraction changes as $\propto |1/y|$ with position y of the Fresnel fringe. The radius of curvature of the present spiral changes with the time of emission t_0 of the secondary waves as given by $|\sqrt{(t-t_0)}/[(t-t_0)^2 - \tau_{cl}^2]|$.

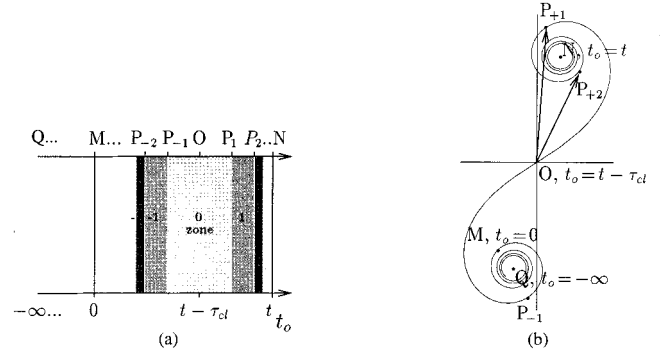


FIG. 4. (a) represents the arrangement of Fresnel zones in time, where t_0 is the time of emission of the secondary wave. The center of the zeroth zone is defined as the emission time of the classical particle propagating with classical velocity. Points Q , M , O , N , and $P_{\pm n}$ correspond to $t_0 = -\infty$, $t_0 = 0$, $t_0 = t - \tau_{cl}$, and $t_0 = t$, and to the boundaries of the zones, respectively. (b) shows the spiral emerging from the graphic addition of the amplitudes of the secondary waves in the complex plane. This spiral is analogous to the famous Cornu spiral of the stationary Fresnel diffraction. If the zones bounded by the point O and the point P_i in (a) are open, the amplitude at the observation point x and time t is proportional to the lengths of the vectors \mathbf{OP}_i in (b). The position of point M in both figures corresponds to the case when $t > \tau_{cl}$.

We denote by Q , M , O , N , and $P_{\pm n}$ the points on the spiral corresponding to $t_0 = -\infty$, $t_0 = 0$, $t_0 = t - \tau_{cl}$, $t_0 = t$, and the boundaries of the zones, respectively. The position of the point M in Figs. 4(a) and 4(b) corresponds to the case when $t > \tau_{cl}$. Although the segment of the spiral between O and N corresponds to the finite time difference τ_{cl} , the point N lies at the focal point. This is a particular feature of Fresnel zones in time. We recall that, in contrast, the focal points of the Cornu spiral for stationary diffraction correspond to the limits $y = \pm\infty$ for the positions of the Fresnel zones.

If the zones bounded by the point O and the point P_i in Fig. 4(a) are open, the amplitude at the observation point x and time t is proportional to the lengths of the vectors \mathbf{OP}_i in Fig. 4b. Due to the well-defined beginning in time of the inhomogeneous boundary condition and the causality principle, only the waves arriving from the open zones within the interval $[0, t]$ are to be taken into account.

Thus for diffraction at the edge in time, i.e., when all zones within $[0, t]$ are open, the following picture emerges (Fig. 5). At $t=0$ the amplitude starts strictly at zero. Subsequently, with increasing time, the amplitude at some fixed space point first increases monotonically in magnitude (M spirals around N) becoming 50% at $t = \tau_{cl}$ (M arrives at O). It continues to increase monotonically until $t = \tau_{cl} + 0.61\sqrt{T\tau_{cl}}$ (we assume again that $T \ll \tau_{cl}$), when M arrives near the lower boundary of the zeroth zone, where it reaches its maximum with 117% of the amplitude of the incident wave. Afterwards the amplitude oscillates in a damped fashion around the amplitude of the incident wave (M spirals into Q). When $t > \tau_{cl}$, setting $t_0^{-n} = 0$ in Eq. (19) gives the number n of maxima at the point x up to the time t as $n = (2/T)(t - \tau_{cl})^2$. This corresponds to the number of loops performed by the point M around the lower focal point Q .

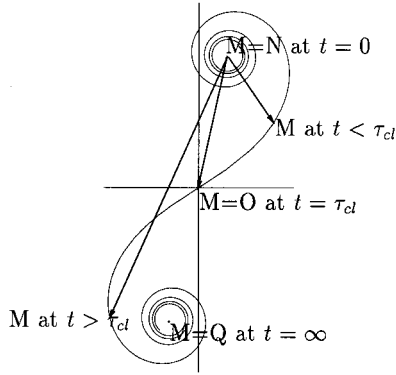


FIG. 5. Diffraction at the edge in time, i.e., all Fresnel zones within $[0, t]$ are open. The length of the vector NM is proportional to the wave amplitude at a fixed position in the course of time. For $t < 0$, the amplitude is equal to zero. With increasing time M begins to spiral around N (the amplitude increases monotonically), then goes through O (at $t = \tau_{cl}$ the amplitude is 50% of the amplitude of the stationary solution). With time increasing further the point M arrives near the lower boundary of the zeroth zone, where the amplitude reaches its maximum of 117% of the amplitude of the stationary solution; afterwards M finally spirals into Q , the stationary solution point, and hence the amplitude oscillates in a damped fashion around the amplitude of the stationary solution.

The close analogy of the Fresnel zone construction in time with the familiar one in space in the stationary case suggests that one may find in the nonstationary optics of matter waves counterparts in time of the familiar diffraction patterns and devices appearing in stationary optics. For example, if we select an arbitrary zeroth zone, construct the position of other zone boundaries in accordance with Eq. (18), and then close all odd zones, all waves arriving from the open even zones at a fixed-space position interfere constructively. Proper temporal modulation of the beam of particles could serve to implement the closing and opening of the Fresnel zones in time. Thus we obtain a device which we call a temporal Fresnel lens. On the other hand, to produce constructive interference at some given position at time t , we can find zones in time according to Eq. (19) and leave only even zones open. The longer the chosen time t is, the more zones contribute to interference, resulting in higher intensities.⁵

IV. DIFFRACTION IN SPACE AND IN TIME

In this section we consider in detail a semi-infinite monochromatic matter wave traveling in the x direction incident on a screen located in the plane $x=0$ which contains a time-dependent single or double-slit opening. We assume the length (along z) of the slit to be infinite, while the time

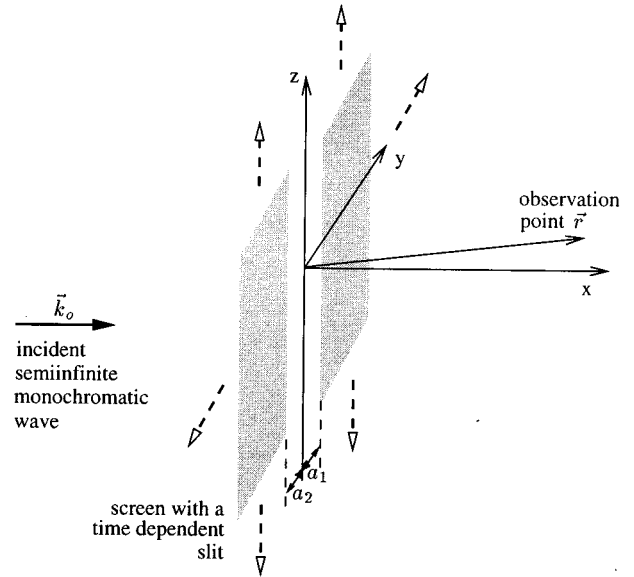


FIG. 6. A scheme of an experiment for observation of both diffraction in space and diffraction in time. An incident semi-infinite monochromatic wave is falling onto an infinitely long slit. The time-varying slit is defined by the width functions $a_1(t)$ and $a_2(t)$. Diffraction effects are observed in the half-space at the right of the screen.

varying width along the y axis is given by functions $a_1(t) \geq 0$ and $a_2(t) \geq 0$ (Fig. 6) for the single slit. The two-dimensional nature of the problem permits us to discuss simultaneously spatial and time diffraction effects. Assuming that the slit is kept shut for $t < 0$ and that the screen is totally nontransmitting, the wave function in the half-space to the right of the screen vanishes for $t < 0$. We shall compute the probability to find a particle at a point in the right half-space at time $t \geq 0$ using the boundary condition approach. Let a slit be opened for a given time and then closed again. We note that it is easy to show that the resulting chopped wave evolving under the homogeneous Dirichlet boundary condition in the plane of the screen can be expressed as a sum of the freely evolving packet and one reflected by the screen. Thus the mathematical assumption of a homogeneous Dirichlet condition at the screen is equivalent to the physical assumption of *perfect reflectivity* of the screen. As expected, the normal component $j_x(\mathbf{r}, t) \equiv (\hbar/2im)(\psi^*(\mathbf{r}, t)[\partial\psi(\mathbf{r}, t)/\partial x] - \psi(\mathbf{r}, t)[\partial\psi^*(\mathbf{r}, t)/\partial x])$ of the probability current vanishes at the screen.⁶ Therefore the total probability in either half-space remains constant when the slit is closed.

We return to our problem. At the slit determined by $x=0$ and $-a_2(t) \leq y \leq a_1(t)$, we assume the inhomogeneous Dirichlet condition $\psi(0, y, z, t) = e^{-i\omega_0 t}$. Our Green's function is again that of Eq. (10). Thus from Eq. (11) we obtain

⁵Recently progress was made in nonstationary optics of atoms by Dalibard's group. Arndt *et al.* [11] used a time-modulated light wave as an atomic mirror to focus different velocity classes of atoms originating from a point source, and to demonstrate the formation of images of a point source. This is an alternative application of the Fresnel lens concept in time to atom optics.

⁶As a matter of fact, if the boundary condition is a general homogeneous one, $\mu(x)\psi(x, t) + \nu(x)[\partial\psi(x, t)/\partial x] = 0$, the absence of the probability flow at the boundary surface still holds when $\mu(x)$ and $\nu(x)$ are real functions. When $\nu(x) = 0$, the condition is of the homogeneous Dirichlet type, and when $\mu(x) = 0$, it is of Neumann type.

$$\psi(\mathbf{r}, t) = \frac{1}{4\pi} \int_0^{t^+} dt_0 \int_{-a_2(t_0)}^{a_1(t_0)} dy_0 \int_{-\infty}^{\infty} dz_0 \\ \times \psi(0, y_0, z_0, t_0) \left. \frac{\partial G(\mathbf{r}, t, \mathbf{r}_0, t_0)}{\partial x_0} \right|_{x_0=0}.$$

Inserting the Green's function and using the chosen boundary condition leads to

$$\psi(\mathbf{r}, t) = -\frac{imx}{2\pi\hbar} \left(\frac{m}{2\pi i\hbar} \right)^{1/2} \int_0^{t^+} dt_0 \frac{1}{(t-t_0)^{3/2}} \\ \times e^{-i\omega_0 t_0} e^{imx^2/2\hbar(t-t_0)} \int_{-a_1(t_0)}^{a_2(t_0)} dy_0 \\ \times e^{im(y-y_0)^2/2\hbar(t-t_0)} \int_{-\infty}^{\infty} dz_0 e^{im(z-z_0)^2/2\hbar(t-t_0)}.$$

After substituting $u = \sqrt{m/\pi\hbar}(t-t_0)(y-y_0)$ and $v = \sqrt{m/\pi\hbar}(t-t_0)(z-z_0)$ for the variables in the spatial integrals, one obtains a solution involving Fresnel integrals,

$$\psi(\mathbf{r}, t) = -\frac{ix}{2} \left(\frac{m}{\pi\hbar} \right)^{1/2} \int_0^{t^+} dt_0 \frac{1}{(t-t_0)^{3/2}} \\ \times e^{-i\omega_0 t_0} e^{imx^2/2\hbar(t-t_0)} \left\{ F \left[\left(\frac{m}{\pi\hbar(t-t_0)} \right)^{1/2} \right. \right. \\ \left. \left. \times [y + a_1(t_0)] \right] - F \left[\left(\frac{m}{\pi\hbar(t-t_0)} \right)^{1/2} [y - a_2(t_0)] \right] \right\}. \quad (20)$$

We notice that the Fresnel integrals depend linearly on the spatial coordinate y , as in stationary Fresnel diffraction. But it is very important to realize that in general it is not possible to separate space and time in solution (20).

From now on we restrict ourselves to the three simplest nontrivial two-dimensional cases: (a) a step-function edge opening (edge opening instantaneously), (b) a square pulse slit opening (slit opening and closing instantaneously), and (c) two square pulse slit openings. For the latter two cases we will consider both spatial single- and double-slit openings in the screen.

Being interested in experimentally observing the phenomena predicted here, we shall discuss as an example in the following subsections a beam of Li-7 atoms with atom mass $m = 7 \times 1.66 \times 10^{-27}$ kg moving with the classical velocity $v_0 = 1$ m/s. The corresponding wavelength and wave period of the de Broglie wave are $\lambda = 5.70 \times 10^{-8}$ m and $T = 1.14 \times 10^{-7}$ s, respectively.

A. Edge in space and in time

In this subsection we consider diffraction at the edge in space and in time, i.e., we let the slit width be determined by the step function in space and in time,

$$a_2(t) = \begin{cases} 0 & \text{for } t < 0 \\ \infty & \text{for } t \geq 0, \end{cases} \\ a_1(t) = 0, \quad \forall t.$$

Kamesberger and Zeilinger [6] reported figures based on the numerical solution of this problem. In order to find an exact relation between diffraction in space and diffraction in time, we now compute the analytical solution. Inserting the slit width functions just defined and changing the integration variable $\tau = t - t_0$ in Eq. (20), we obtain

$$\psi^{\text{edge}}(\mathbf{r}, t) = -\frac{ix}{2} \left(\frac{m}{\pi\hbar} \right)^{1/2} e^{-i\omega_0 t} \int_0^t d\tau \frac{1}{\tau^{3/2}} \\ \times e^{i\omega_0 \tau} e^{imx^2/2\hbar\tau} \left\{ F[\infty] - F \left[\left(\frac{m}{\pi\hbar\tau} y \right)^{1/2} \right] \right\}. \quad (21)$$

In our analysis of this equation we will consider three different spatial regions.

1. Geometric shadow

If $\sqrt{m/\pi\hbar}ty \gg 1$, $F[\sqrt{m/\pi\hbar}\tau y]$ can be substituted by its asymptotic behavior [11] $F[z \rightarrow \infty] = F[\infty] + (e^{i\pi z^2/2}/i\pi z) + O[z^{-3}]$ with an error of the order of $(\sqrt{m/\pi\hbar}\tau y)^{-3}$. For the atomic beam parameters introduced above, this criterion is satisfied for $y \gg 10^{-4}$ m at an observation time $t = 1$ s. With that approximation, we obtain

$$\psi^{\text{shadow}}(\mathbf{r}, t) = \frac{1}{2\pi} \frac{x}{y} e^{-i\omega_0 t} \int_0^t d\tau \frac{1}{\tau} e^{i\omega_0 \tau} e^{im(x^2+y^2)/2\hbar\tau}.$$

The main contribution to the integral comes from times around the classical time $\tau_{cl_1} \equiv m\sqrt{x^2+y^2}/k_0\hbar$, where the phase of the integrand is stationary. Treating the function $\tau^{1/2}$ to be constant in comparison with the rapidly varying exponential integrands, we approximate $1/\tau \approx \tau^{1/2}/\tau^{3/2} \approx \tau_{cl_1}^{1/2}/\tau^{3/2}$.

Then, with the substitution $\xi = 1/\sqrt{\tau}$, we find

$$\psi^{\text{shadow}}(\mathbf{r}, t) = \frac{1}{\pi} \frac{x}{y} \left(\frac{m\sqrt{x^2+y^2}}{k_0\hbar} \right)^{1/2} e^{-i\omega_0 t} \int_{1/\sqrt{t}}^{\infty} d\xi \\ \times e^{i\omega_0/\xi^2} e^{[im(x^2+y^2)/2\hbar]\xi^2}.$$

Again using solution (13) from the integral tables, the final solution is a sum of two waves corresponding to initial waves $e^{ik_0 x} \theta[-x]$ and $e^{-ik_0 x} \theta[-x]$. However, in the limit $\sqrt{x^2+y^2} \gg \lambda$ the contribution of the latter one propagating to the left vanishes, leaving

$$\psi^{\text{shadow}}(\mathbf{r}, t) = \frac{1}{2\pi} \frac{x}{y} \frac{1}{\sqrt{k_0\sqrt{x^2+y^2}}} e^{i(k_0\sqrt{x^2+y^2} - \omega_0 t)} \\ \times \left(F \left[\frac{2}{\sqrt{Tt}} (t - \tau_{cl_1}) \right] - F[-\infty] \right). \quad (22)$$

Transforming solution (22) into polar coordinates, $\tan\alpha \equiv y/x$ and $\rho \equiv \sqrt{x^2+y^2}$, one may easily recognize a kind of cylindrical wave going out from the edge (Fig. 7), $\psi^{\text{shadow}}(\mathbf{r}, t) = (1/2\pi)(1/\tan\alpha)(1/\sqrt{k_0\rho}) e^{i(k_0\rho - \omega_0 t)} [F((2/\sqrt{Tt})[t - (m\rho/k_0\hbar)]) - F[-\infty]]$. If $\rho \rightarrow \infty$ and/or $\alpha \rightarrow \pi/2$, we obtain $\psi(\mathbf{r}, t) \rightarrow 0$, as is to be expected deep in the geometric shadow.

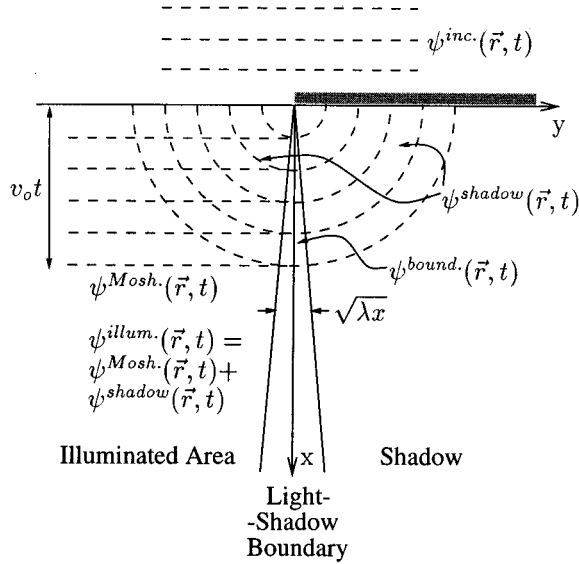


FIG. 7. Schematic view of diffraction at the edge both in space and in time indicating particular space regions. The solution inside the geometric shadow $\psi^{\text{shadow}}(\mathbf{r}, t)$ is a product between the solutions of diffraction at the edge in space and of diffraction at the edge in time. The solution $\psi^{\text{illum.}}(\mathbf{r}, t)$ in the geometric illuminated region is a superposition of a scattered wave $\psi^{\text{shadow}}(\mathbf{r}, t)$ and $\psi^{\text{Mosh.}}(\mathbf{r}, t)$ evolving freely from the incident wave. The solution at the light-shadow boundary $\psi^{\text{bound.}}(\mathbf{r}, t)$ is a product of a stationary solution of the diffraction at an edge in space describing a transitional region from the geometric shadow to the geometric illuminated region and the solution of diffraction at the edge in time.

Solution (22) is a product between the solution for the stationary diffraction into the geometric shadow and the solution of diffraction at the edge in time (15), involving here the classical time $\tau_{\text{cl}_1} = m\sqrt{x^2 + y^2}/k_0\hbar$. An analysis similar to the one carried out for Moshinsky's problem (see Fig. 2) can be given here. Thus the intensity level at two distinctive points, at the classical time and at the first maximum in time, is 25% and 137%, respectively, of the stationary intensity in the geometric shadow (the stationary solution is $\lim_{t \rightarrow \infty} \psi^{\text{shadow}}(\mathbf{r}, t) = (1/\sqrt{2}\pi)e^{i(\pi/4)}(x/y)[1/(k_0\sqrt{x^2 + y^2})^{1/2}]e^{i(k_0\sqrt{x^2 + y^2} - \omega_0 t)}$). The width in time of the transitional interval is of the order of $\sqrt{T\tau_{\text{cl}_1}}$. With the atomic wave data assumed above, the transitional time at $\sqrt{x^2 + y^2} \approx 1\text{ m}$ is approximately $3.4 \times 10^{-4}\text{ s}$. Solution (22) is accurate up to the order of $(x/k_0 y^2)^{3/2}$. The intensity distribution of diffracted cold neutrons of $\lambda = 20\text{ \AA}$ behind the edge is given in Fig. 8.

2. Geometric illuminated region

Setting (compare the case of the geometric shadow) $\sqrt{m/\pi\hbar}ty \ll -1$ and using the asymptotic behavior [12] $F[z \rightarrow -\infty] = F[-\infty] + (e^{i\pi z^2/2}/i\pi z) + O[z^{-3}]$, we approximate Fresnel's integral in Eq. (21) up to the order of $(\sqrt{m/\pi\hbar}\tau y)^{-3}$ and evaluate

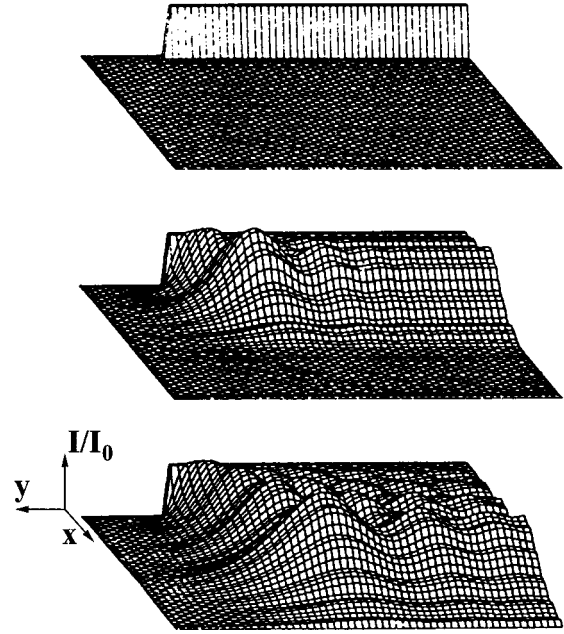


FIG. 8. Diffraction at the edge both in space and in time. Cold neutrons of wavelength $\lambda = 20\text{ \AA}$ propagating in the positive- x direction are incident on a screen located at $x=0$. There, along the negative- y direction, the edge is opened instantaneously at the time $t=0$. The figure shows the numerically calculated intensity distribution at times $t=0, 39,$ and 78 ps , respectively, from top to bottom (from Ref. [6]).

$$\begin{aligned} \psi^{\text{illum.}}(\mathbf{r}, t) &= x \left(\frac{m}{2\pi\hbar} \right)^{1/2} e^{-i(\pi/4)} e^{-i\omega_0 t} \int_0^t d\tau \frac{1}{\tau^{3/2}} \\ &\quad \times e^{i\omega_0 \tau} e^{imx^2/2\hbar\tau} + \psi^{\text{shadow}}(\mathbf{r}, t) \\ &= \psi^{\text{Mosh.}}(\mathbf{r}, t) + \psi^{\text{shadow}}(\mathbf{r}, t). \end{aligned} \quad (23)$$

Here we again neglect the contribution of the wave propagating to the left. The first term is exactly Moshinsky's solution (15), the one which would be present if there were no edge in space. In that sense $\psi^{\text{shadow}}(\mathbf{r}, t)$ is a correction to geometric optics (Fig. 7). Since the solution in the geometric illuminated region is a superposition of a freely evolving wave $\psi^{\text{Mosh.}}(\mathbf{r}, t)$ involving the classical time $\tau_{\text{cl}} = mx/k_0\hbar$ and a scattered wave $\psi^{\text{shadow}}(\mathbf{r}, t)$ involving the classical time $\tau_{\text{cl}_1} = m\sqrt{x^2 + y^2}/k_0\hbar$, $\psi^{\text{illum.}}(\mathbf{r}, t)$ is not a product of the stationary solution in the illuminated region and one of diffraction at the edge in time. Going away from the edge (in polar coordinates $\rho \rightarrow \infty$) the solution reduces to Moshinsky's. The obtained solution (23) is correct up to errors of the order of $(x/k_0 y^2)^{3/2}$.

3. Light-shadow boundary

If $|\sqrt{m/\pi\hbar}ty| \leq 1$, we divide the integration region into two parts:

$$\begin{aligned} \psi^{\text{bound.}}(\mathbf{r}, t) = & -\frac{ix}{2} \left(\frac{m}{\pi\hbar} \right)^{1/2} e^{-i\omega_0 t} \left(\int_0^{\bar{\tau}} d\tau \frac{1}{\tau^{3/2}} e^{i\omega_0 \tau} \right. \\ & \times e^{imx^2/2\hbar\tau} \left\{ F[\infty] - F \left[\left(\frac{m}{\pi\hbar\tau} \right)^{1/2} y \right] \right\} \\ & + \int_{\bar{\tau}}^t d\tau \frac{1}{\tau^{3/2}} e^{i\omega_0 \tau} e^{imx^2/2\hbar\tau} \\ & \left. \times \left\{ F[\infty] - F \left[\left(\frac{m}{\pi\hbar\tau} \right)^{1/2} y \right] \right\} \right), \end{aligned}$$

where $\bar{\tau} \equiv my^2/\pi\hbar$. The first integral can be further evaluated as in the case of the geometric shadow (if $y < 0$) or the geometric illuminated region (if $y > 0$). If $\bar{\tau} \lesssim \tau_{\text{cl}}$, which is equivalent to $|y| \lesssim (1/\sqrt{2})\sqrt{\lambda x}$, the main contribution to the second integral comes from that region around τ_{cl} where the phase of the integrand is stationary. Taking again our Li-atom example with $x \approx 1\text{ m}$, y lies in the interval $|y| \lesssim 10^{-4}\text{ m}$, not considered so far. Within the integration interval $[\bar{\tau}, t]$, where $|\sqrt{m/\pi\hbar}\tau y| < 1$ the term $F[\infty] - F[\sqrt{m/\pi\hbar}\tau y]$ has as its asymptotic limit $F[\infty] - F[z \rightarrow 0] = F[\infty] - z - (i\pi z^3/6) - O[z^5]$ [12]. Due to its slowly varying behavior compared with other integrands, we treat this term as being the constant $F[\infty] - F[\sqrt{m/\pi\hbar}\tau_{\text{cl}}y]$ in the integration interval. Thus we obtain

$$\begin{aligned} \psi^{\text{bound.}}(\mathbf{r}, t) = & -\frac{i}{2} e^{i(k_0 x - \omega_0 t)} \left\{ F[\infty] - F \left[\left(\frac{2}{\lambda x} \right)^{1/2} y \right] \right\} \\ & \times \left(F \left[\frac{2}{\sqrt{T}t} (t - \tau_{\text{cl}}) \right] - F \left[\frac{2}{\sqrt{T}\bar{\tau}} (\bar{\tau} - \tau_{\text{cl}}) \right] \right) \\ & + \begin{cases} \psi^{\text{illum.}}(\mathbf{r}, \bar{\tau}) & \text{for } y < 0 \\ \psi^{\text{shadow}}(\mathbf{r}, \bar{\tau}) & \text{for } y > 0. \end{cases} \quad (24) \end{aligned}$$

In the limit when the argument of the fourth Fresnel integral $(2/\sqrt{T}\bar{\tau})(\bar{\tau} - \tau_{\text{cl}}) = (2/y)\sqrt{m/\pi\hbar}T[y^2 - (\lambda x/2)]$ goes to negative infinity, and consequently $\psi^{\text{illum.}}(\mathbf{r}, \bar{\tau})$ and $\psi^{\text{shadow}}(\mathbf{r}, \bar{\tau})$ tend to zero, solution (24) becomes

$$\begin{aligned} \psi^{\text{bound.}}(\mathbf{r}, t) = & -\frac{i}{2} e^{i(k_0 x - \omega_0 t)} \left\{ F[\infty] - F \left[\left(\frac{2}{\lambda x} \right)^{1/2} y \right] \right\} \\ & \times \left(F \left[\frac{2}{\sqrt{T}t} (t - \tau_{\text{cl}}) \right] - F[-\infty] \right). \quad (25) \end{aligned}$$

Since in our Li-atom example $(2/y)\sqrt{m/\pi\hbar}T[y^2 - (\lambda x/2)] \approx 10^{10}[y^2 - (\lambda x/2)]$, the above condition is satisfied for a wide range of y within the interval considered $|y| \lesssim (1/\sqrt{2})\sqrt{\lambda x}$. Due to the fact that $\psi^{\text{bound.}}(\mathbf{r}, t)$ is the product of solution (15) of the diffraction at the edge in time and the one of stationary edge diffraction, the wave modulation is the strongest in the light-shadow boundary region (see Fig. 8). Thus, on the one hand, the intensity at the classical cutoff at $y=0$ at time $t = \tau_{\text{cl}}$ is only $0.0625 (=0.25^2)$ of the intensity of the incident wave. On the other hand, the product of the intensities of the first stationary maximum in space at $y = 0.87\sqrt{\lambda x}$ and the first maximum in time at $t = \tau_{\text{cl}}$

+ $0.61\sqrt{T}\tau_{\text{cl}}$ (here we assume again that $T \ll \tau_{\text{cl}}$) is $1.88 (=1.37^2)$ of the intensity of the incident wave. This significantly exceeds the first maxima in time in other spatial regions even in the geometrically illuminated one.

Keeping the time fixed and going from the geometric shadow to the illuminated area, or keeping a point in space fixed and going from times $t < \tau_{\text{cl}}$ to times $t > \tau_{\text{cl}}$, the intensity in both cases increases monotonically, and after it exhibits a maximum it begins to oscillate in a damped fashion. The widths of the transitional regions where the space shadow (Fig. 7) and time shadow are washed out are, for $\sqrt{x^2 + y^2} \gg \lambda$, approximately $\sqrt{\lambda x}$ and $\sqrt{T}\tau_{\text{cl}}$, respectively. For the Li-atom parameters in our example the transitional spatial region is $2.4 \times 10^{-4}\text{ m}$ at $x = 1\text{ m}$ and the transitional time interval is $3.4 \times 10^{-4}\text{ s}$ at $t = 1\text{ s}$. Expression (24) connects the solution for the light-shadow boundary with the ones for the geometric illuminated region and for the geometric shadow.

Expressing the final solutions (22), (23), and (25) through classical variables (through the classical velocity v_0 instead of k_0 and ω_0) and taking the classical limit ($\hbar \rightarrow 0$ and/or $m \rightarrow \infty$) we find $\psi^{\text{edge}}(\mathbf{r}, t) \rightarrow e^{i(x - v_0 t)} \theta[t - (x/v_0)] \theta[-y]$. As expected, this solution neither shows diffraction in space nor in time.

The effects of diffraction in space and in time discussed here are rather small for our assumed atom example. However they can be increased significantly in the case of diffraction at a slit in space with a width of the order of the wavelength, and a slit in time with a pulse length of the order of the wave period, as will be considered next.

B. Single slit in space and in time

In this subsection we consider diffraction at a single slit both in space and in time, i.e., the slit width is given by a square function both in space and in time:

$$a_1(t) = a_2(t) = \begin{cases} \frac{a}{2} & \text{for } 0 \leq t \leq T_{\text{ch}} \\ 0 & \text{for } t < 0, t > T_{\text{ch}}, \end{cases}$$

where T_{ch} is the chop time. In an earlier solution [4,5] of the present problem involving Neumann boundary conditions, the computation was performed with the method of stationary phase. This method consists of replacing the phase function (see Fig. 3) by a parabola centered at the classical time. Such a removal of the asymmetry effects of the phase function is sufficient for the evolution of ‘‘nearly classical’’ packets which are chopped with a pulse duration $T_{\text{ch}} \gg T$. The problem of chopping a beam with a pulse duration short enough to affect the energy spectrum of the beam was discussed by Felber *et al.* [7]. Again using Neumann conditions, these authors concentrated on a triangular slit pulse opening additionally involving a modulation of the energy spectrum associated with a motion of the slit edges with finite velocity.

In order to emphasize the close relation between diffraction patterns in space and in time, we now choose slit opening functions which have equal space and time dependencies. Furthermore we use the Dirichlet condition whose interpretation is physically clear as discussed in Sec. III A (the in-

homogeneous Dirichlet condition) and at the beginning of the Sec. IV (the homogeneous Dirichlet condition).

Applied to our example, conditions for simultaneous strong diffraction in space $\lambda \approx a$ and in time $T \approx T_{\text{ch}}$ require a slit width $a \approx 10^{-7}$ m and simultaneously a chop time $T_{\text{ch}} \approx 10^{-7}$ s. We shall assume in the discussions of our example just these experimentally realizable values for the slit width and chop time.

With the slit opening function given above and substituting $\tau = t - t_0$, Eq. (20) transforms to

$$\begin{aligned} \psi^{\text{slit}}(\mathbf{r}, t) = & -\frac{ix}{2} \left(\frac{m}{\pi\hbar} \right)^{1/2} e^{-i\omega_0 t} \int_{\tau-T_{\text{ch}}}^t d\tau \frac{1}{\tau^{3/2}} e^{i\omega_0 \tau} \\ & \times e^{imx^2/2\hbar\tau} \left\{ F \left[\left(\frac{m}{\pi\hbar\tau} \right)^{1/2} \left(y + \frac{a}{2} \right) \right] \right. \\ & \left. - F \left[\left(\frac{m}{\pi\hbar\tau} \right)^{1/2} \left(y - \frac{a}{2} \right) \right] \right\}. \end{aligned} \quad (26)$$

Let us assume that

$$\left(\frac{m}{\pi\hbar(t-T_{\text{ch}})} \right)^{1/2} \frac{a}{2} \ll 1. \quad (27)$$

In our example this criterion is satisfied to within 10^{-4} for the observation time $t = 1$ s. For $\Delta z \ll z$ we can approximate $F[z + \Delta z] - F[z] \approx (2/\pi z) \sin(\Delta z \pi/2) e^{i(\pi/2)z^2}$ with $\Delta z = \sqrt{m/\pi\hbar\tau} a$ and $z = \sqrt{m/\pi\hbar\tau} y$. Then it follows that

$$\begin{aligned} \psi^{\text{slit}}(\mathbf{r}, t) = & -\frac{ix}{\pi y} e^{-i\omega_0 t} \int_{t-T_{\text{ch}}}^t d\tau \frac{1}{\tau} \\ & \times e^{i\omega_0 \tau} e^{im(x^2+y^2)/2\hbar\tau} \sin \frac{may}{2\hbar\tau}. \end{aligned} \quad (28)$$

It should be noticed that the dependence on the spatial coordinate y in one of the integrands is of the form $\sin[cy]/cy$ as in the stationary Fraunhofer diffraction.

The phase of the integrand in Eq. (28) is a very rapidly varying function of time with a stationary region around the classical time $\tau_{\text{cl}} \equiv m\sqrt{x^2+y^2}/k_0\hbar$. Yet, due to the possible strong spreading of the wave packet after chopping, the stationary phase method could not be usefully employed, since, for many space points where the probability at a given time significant differs from zero, the integration interval does not contain the classical time. Obviously a more precise calculation, valid for a wider class of solutions, can be performed if we expand the phase of the integrand not around the classical time but around the center $t - (T_{\text{ch}}/2)$ of the integration interval [7]. This method will be applied in the present paper, and solutions for nearly classical packets obtainable with the stationary phase method will be obtained in the limit.

In order to separate the dependence on the y direction from the time integral in Eq. (28), we approximate

$$\frac{mayT_{\text{ch}}/2}{2\hbar[t - (T_{\text{ch}}/2)]^2} \rightarrow 0. \quad (29)$$

Within approximation (29) the function $1/\tau$ in the argument of the sine function in Eq. (28) can be expanded to zeroth order around the center $t - (T_{\text{ch}}/2)$ of the integration interval $[t - T_{\text{ch}}, t]$. This means that the influence of the finite chop duration on the $\sin[cy]/cy$ dependence is insignificant. In our atom example, expression (29) is of the order of 10^{-7} at the observation time $t = 1$ s and within the region around $x \approx 1$ m where the particle is found with high probability. Obviously it is meaningful to test the conditions for the validity of approximations only for those space points where, for a given observation time, the probability density to find the particle differs significantly from zero. These points could be assumed to be within the region inside the first few minima along the x and y axes, whose existence we shall prove later. Naturally, the size of that area depends both on the chop time and on the slit width; a shorter chop time T_{ch} and/or a smaller slit width a cause stronger wave packet spreading.

With the approximation mentioned above, the solution

$$\begin{aligned} \psi^{\text{slit}}(\mathbf{r}, t) = & -\frac{ix}{\pi y} e^{-i\omega_0 t} \sin \frac{may}{2\hbar[t - (T_{\text{ch}}/2)]} \\ & \times \int_{t-T_{\text{ch}}}^t d\tau \frac{1}{\tau} e^{i\omega_0 \tau} e^{im(x^2+y^2)/2\hbar\tau} \end{aligned} \quad (30)$$

becomes a product of two terms. The first one we recognize as the Fraunhofer limit of the diffraction in space at a certain observation time, and the second term, the time integral, as the diffraction in time observed at a certain point in space. Exactly speaking, this is not quite appropriate, since these terms do not depend separately on the y coordinate and on time. It should be emphasized that solution (30) is not a product of the stationary solution of diffraction at a spatial slit in Fraunhofer limit (of the form $\propto [\sin(k_0 ay/2x)] / (k_0 ay/2x)$) and a one-dimensional solution of diffraction at the slit in time (involving time and the direction of propagation x).

In order to transform the time integral in Eq. (30) into the Fresnel integrals, we take the limit

$$\frac{m(x^2+y^2)(T_{\text{ch}}/2)^3}{2\hbar[t - (T_{\text{ch}}/2)]^4} \rightarrow 0, \quad (31)$$

and proceed by expanding the function $1/\tau$ in the argument of the exponential function in Eq. (30) around $t - (T_{\text{ch}}/2)$, retaining terms up to the second order. In our example criterion (31) is satisfied up to order 10^{-14} . Compared to the other rapidly varying functions the integrand function $1/\tau$ in Eq. (30) can be treated as a constant $1/(t - T_{\text{ch}}/2)$ within a sufficiently short integration interval $[t - T_{\text{ch}}, t]$. The approximations mentioned and the substitution

$$\begin{aligned} w = & \left(\frac{m(x^2+y^2)}{\pi\hbar[t - (T_{\text{ch}}/2)]^3} \right)^{1/2} \left[\tau - \frac{3}{2} \left(t - \frac{T_{\text{ch}}}{2} \right) \right. \\ & \left. + \frac{\hbar\omega_0[t - (T_{\text{ch}}/2)]^3}{m(x^2+y^2)} \right] \end{aligned}$$

lead to an expression including Fresnel integrals:

$$\begin{aligned}
\psi^{\text{slit}}(\mathbf{r}, t) = & -\frac{ix}{y} \left(\frac{\hbar[t - (T_{\text{ch}}/2)]^{1/2}}{\pi m(x^2 + y^2)} \right) e^{i(\omega_0 t/2)} e^{-i(3\omega_0 T_{\text{ch}}/4)} \\
& \times e^{i(3m(x^2 + y^2)/8\hbar[t - T_{\text{ch}}/2])} \\
& \times e^{-i(\hbar\omega_0^2[t - (T_{\text{ch}}/2)]^3/2m(x^2 + y^2))} \\
& \times \sin \frac{may}{2\hbar[t - (T_{\text{ch}}/2)]} \\
& \times \left(F \left[\left(\frac{m(x^2 + y^2)}{\pi\hbar[t - (T_{\text{ch}}/2)]^3} \right)^{1/2} \left[t - \frac{3}{2} \left(t - \frac{T_{\text{ch}}}{2} \right) \right. \right. \right. \\
& \left. \left. \left. + \frac{2\hbar\omega_0[t - (T_{\text{ch}}/2)]^3}{m(x^2 + y^2)} \right] \right) \right. \\
& \left. - F \left[\left(\frac{m(x^2 + y^2)}{\pi\hbar[t - (T_{\text{ch}}/2)]^3} \right)^{1/2} \left[t - T_{\text{ch}} - \frac{3}{2} \left(t - \frac{T_{\text{ch}}}{2} \right) \right. \right. \right. \right. \\
& \left. \left. \left. + \frac{2\hbar\omega_0[t - (T_{\text{ch}}/2)]^3}{m(x^2 + y^2)} \right] \right] \right). \quad (32)
\end{aligned}$$

We can again understand solution (32) as a product of two terms, representing Fraunhofer diffraction in space at a fixed observation time and Fresnel diffraction in time at a fixed observation point in space.

Assuming the condition

$$\left(\frac{m(x^2 + y^2)}{\pi\hbar[t - (T_{\text{ch}}/2)]^3} \right)^{1/2} T_{\text{ch}} \ll 1, \quad (33)$$

one may also introduce the Fraunhofer limit of diffraction in time at a certain observation point in space:

$$\begin{aligned}
\psi^{\text{slit}}(\mathbf{r}, t) = & -\frac{i2}{\pi} \frac{x}{y} \frac{1}{\omega_0[t - (T_{\text{ch}}/2)]} \\
& \times \frac{1}{1 - m(x^2 + y^2)/2\hbar\omega_0[t - (T_{\text{ch}}/2)]^2} \\
& \times \sin \frac{may}{2\hbar[t - (T_{\text{ch}}/2)]} \\
& \times \sin \left[\frac{\omega_0 T_{\text{ch}}}{2} \left(1 - \frac{m(x^2 + y^2)}{2\hbar\omega_0[t - (T_{\text{ch}}/2)]^2} \right) \right] \\
& \times e^{-i\omega_0(T_{\text{ch}}/2)} e^{im(x^2 + y^2)/2\hbar[t - (T_{\text{ch}}/2)]}. \quad (34)
\end{aligned}$$

Thus, now, our solution is a product of two terms describing the Fraunhofer diffraction in space at a certain observation time, and the Fraunhofer diffraction in time at a certain observation point in space. In our standard atom example, approximation (33) is of the order of 10^{-4} .

Solution (34) just evaluated deserves some comments. First, it is to be expected that solution (34) for short chop times and small slit widths approaches the effect of a disturbance due to a line of point dipoles extended uniformly along z_0 axes. This effect can be calculated as a superposition of contributions of individual dipole sources lying on the z_0 axis: $-(1/4\pi) \int_{-\infty}^{\infty} dz_0 |\nabla_0 G(\mathbf{r}, t, \mathbf{r}_0, t_0)|$

$\propto (x/t^2) e^{im(x^2 + y^2)/2\hbar t}$. It is easy to show that solution (34) transforms into the same expression in the limits $a \rightarrow 0$ and $T_{\text{ch}} \rightarrow 0$.

We note that there are two types of minima. Their positions in space at a certain time are

$$y_{\text{min}} = \frac{2n\pi\hbar[t - (T_{\text{ch}}/2)]}{ma}, \quad n \in \mathbb{Z} \setminus \{0\} \quad (35)$$

and

$$\begin{aligned}
x_{\text{min}}'^2 + y_{\text{min}}'^2 = & v_0^2 \left(t - \frac{T_{\text{ch}}}{2} \right)^2 - \frac{4n'\pi\hbar[t - (T_{\text{ch}}/2)]^2}{mT_{\text{ch}}}, \\
n' \in & \mathbb{Z} \setminus \{0\}, \quad (36)
\end{aligned}$$

respectively, where n and n' are the orders of the minima. For a fixed observation time minima (35) and (36) form lines parallel to the x axis and circles in the x - y planes, respectively, both seen in Figs. 9(a), 10(a), 11(a), and 12(a). On the other hand, for a fixed plane x of observation minima (35) and (36) form lines $y = ct$ and hyperbolas in the y - t planes, respectively, both seen in Figs. 9(b), 10(b), 11(b), and 12(b). If $T_{\text{ch}} < T$, the positions of minima (36) assume complex values for $n' > 0$. Indeed we see in Figs. 9 and 10, representing examples with a chop time shorter than the wave period, that all minima after the central one vanish. The angular separation Eq. (35) between adjacent minima in space of the first kind,

$$\Delta\alpha \equiv 2 \frac{y_{1\text{min}}(t)}{v_0 t} = 2 \frac{\lambda}{a}, \quad (37)$$

is exactly the same as in the stationary case within the Fraunhofer limit. The time independence of the angular separation (37) of minima is in agreement with the fact that the distance between minima (35) and the central maximum increases linearly with time, as seen in Figs. 9(b), 10(b), 11(b), and 12(b).

It should be noted here that in the examples represented in the figures the conditions for the Fraunhofer limit in space and in time will always be satisfied. In the figures the probability is not normalized. In contrast, in order to make it easier to compare the different patterns, the probability density is scaled such that in the case of a single slit both in space and in time with slit width 10^{-6} m and chop time 10^{-6} s (Fig. 12) the central maximum at $t = 1$ s is defined to have the value 1. Now we shall return to our discussion.

A rough estimate of the width of the diffraction pattern as given by the distance between the two first minima in space and in time, respectively, can also be obtained from uncertainty considerations, providing greater physical understanding. The wave constrained by the slit width in the y direction has an uncertainty of momentum in the y direction given by $\Delta p_y a \approx \hbar$. Analogously, the wave constrained by the chop time duration has an uncertainty in energy given by $\Delta E T_{\text{ch}} = (m/2)(\Delta v_x^2 + \Delta v_y^2) T_{\text{ch}} \approx \hbar$. Therefore, we obtain two types of minima $\frac{y_{\pm 1 \text{ min}}}{t} = \pm \Delta p_y / m = \pm (2\pi\hbar t / ma)$ and $\frac{y_{\pm 1 \text{ min}}}{\sqrt{x_{\pm 1 \text{ min}}'^2 + y_{\pm 1 \text{ min}}'^2}} = \pm \sqrt{v_0^2 \pm (\Delta v_x^2 + \Delta v_y^2)} t = \pm \sqrt{v_0^2 \pm (4\pi\hbar / mT_{\text{ch}})} t$, closely related to position-momentum and time-energy uncertainty relations

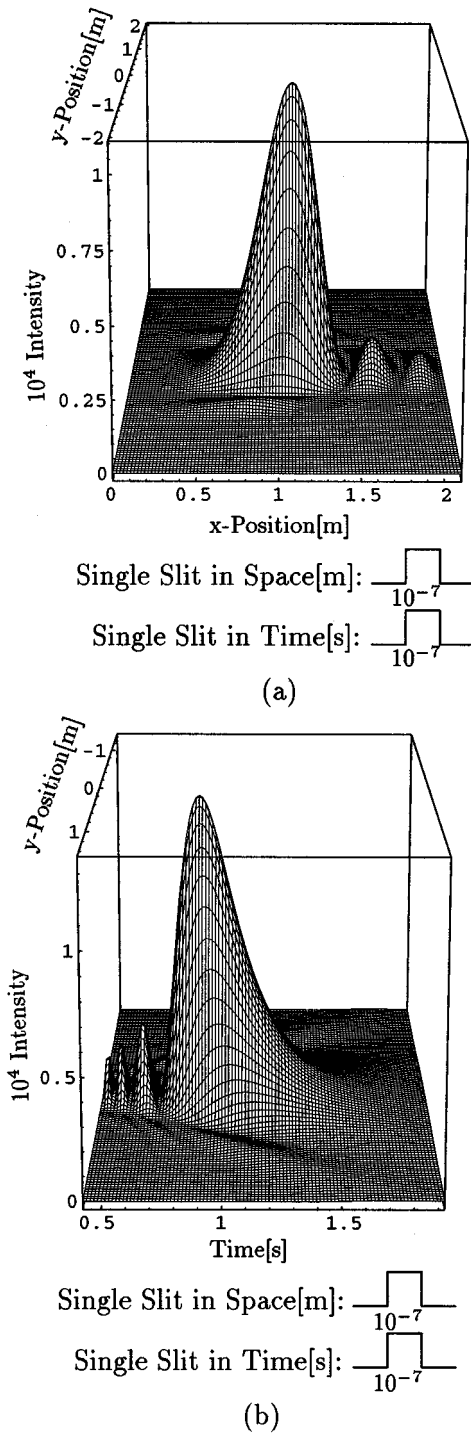


FIG. 9. Diffraction at a single slit both in space and in time. Li-7 atoms propagating in the positive- x direction with the classical velocity $v_0=1$ m/s are incident on a screen located at $x=0$. There, at position $y=0$, a single slit of width 10^{-7} m is instantaneously opened at the time $t=0$ for 10^{-7} s. These numbers are of the same order of magnitude as the de Broglie wavelength $\lambda=5.7\times 10^{-8}$ m and the wave period $T=1.14\times 10^{-7}$ s respectively. (a) shows the wave packet at a time $t=1$ s after the opening and closing of the single slit in time. (b) demonstrates the probability to detect the particle in a fixed detector plane at $x=1$ m as a function of time. It is clearly seen that significant diffraction takes place both in space and in time. It should be mentioned that none of the graphs in Figs. 9–15 is normalized.

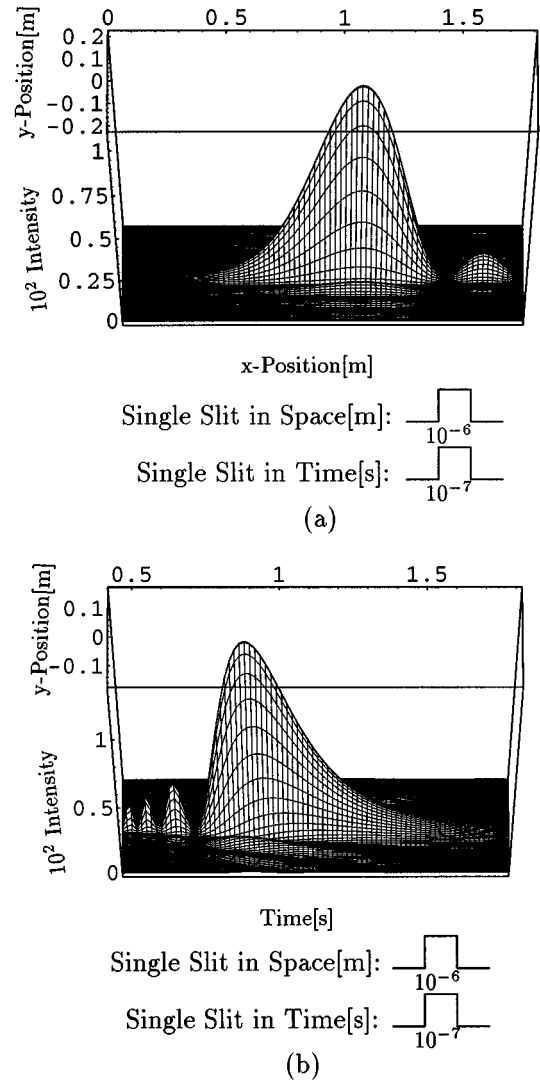


FIG. 10. Same geometry as Fig. 9, but now with the single slit in space having a width of 10^{-6} m, i.e., a slit significantly wider than the de Broglie wavelength. (a) again shows the wave packet after $t=1$ s, and (b) demonstrates the arrival times at the observation plane located at $x=1$ m. It is evident that now the diffraction spreading in space is very small, while the spreading in time is basically the same as in Fig. 9.

respectively. Thus the nonsymmetrical arrangement of the latter minima around $x=v_0t$ is a consequence of the nonlinear dependence of energy on velocity.

Taking chop times which are long compared to the wave period, the mean width of the energy remains narrow after chopping. This permits us to expand such localized packets around the classical time. If, additionally, the slit width and the wavelength are of the same order, a strong spreading of the wave packet along the y direction results, requiring that the classical time $\tau_{cl}=m\sqrt{x^2+y^2}/k_0\hbar$ depends both on x and y dimensions. A wave packet with such experimental parameters is represented in Fig. 11. If, on the contrary, the slit width is wide compared to the wavelength, the y dimension of the wave packet remains smaller than the distance reached along the x direction and the classical time becomes $\tau_{cl}\approx mx/k_0\hbar$. For such a case we assume

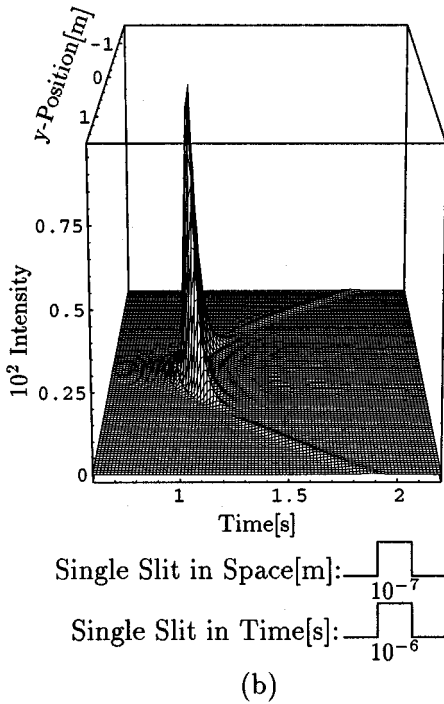
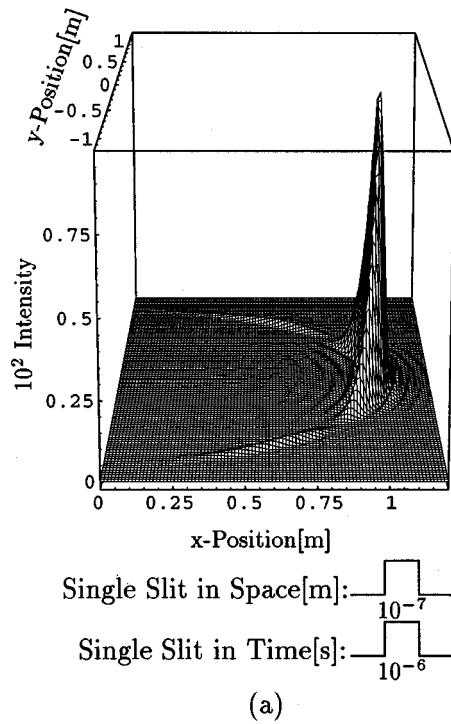


FIG. 11. Again the same geometry as in Figs. 9 and 10, but now with a single slit in space of width 10^{-7} m, i.e., comparable to the de Broglie wavelength and a single slit in time of 10^{-6} s which is much larger than the de Broglie wave period. It is clearly seen that now the diffraction in space is very significant, while the diffraction in time only produces small ripples of the wave packet. The circular spreading in (a) is due to the propagation of a wave with a well-defined speed (close to the classical one $v_0 = 1$ m/s), but an undefined direction of propagation.

$$\frac{3m(x^2 + y^2)}{2\hbar\omega_0} \left(\frac{t - \tau_{cl}}{\tau_{cl}} \right)^2 \ll 1, \quad \frac{m a y}{2\hbar\tau_{cl}} \frac{t - \tau_{cl}}{\tau_{cl}} \ll 1,$$

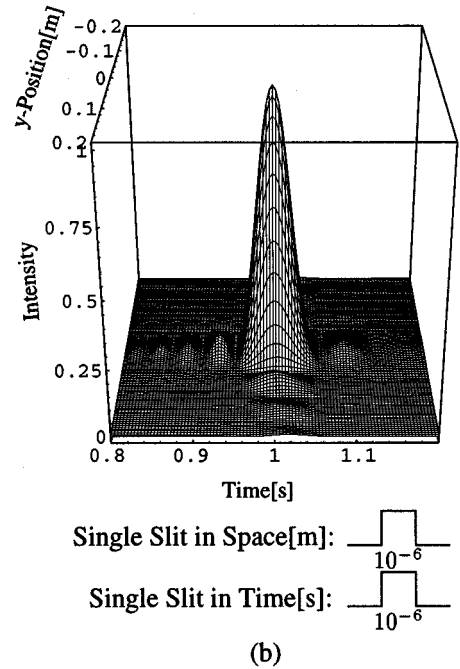
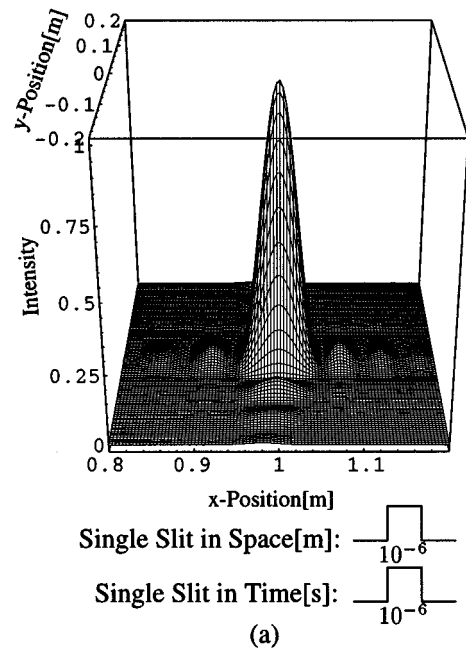


FIG. 12. Diffraction at a single slit in space and a single slit in time, both of which are large compared to the de Broglie wavelength and the wave period. Note the different scale compared to the previous figures. It is clearly seen that now the diffraction phenomena are less pronounced than before, and much more symmetric, indicating the propagation of “nearly classical” packets.

$$\frac{3m(x^2 + y^2)T_{ch}}{4\hbar\tau_{cl}^2} \left(\frac{t - \tau_{cl}}{\tau_{cl}} \right)^2 \ll 1$$

$$\text{and } \frac{m(x^2 + y^2)}{2\hbar\tau_{cl}} \left(\frac{t - \tau_{cl}}{\tau_{cl}} \right)^2 \ll 1 \quad (38)$$

and we approximate expression (34) as

$$\begin{aligned} \psi^{\text{slit}}(\mathbf{r}, t) = & -\frac{i}{\pi} \frac{x}{y} \frac{1}{\omega_0 [t - (T_{\text{ch}}/2) - \tau_{\text{cl}}]} \sin \frac{k_0 a y}{2x} \\ & \times \sin \left[\frac{\omega_0 T_{\text{ch}}}{\tau_{\text{cl}}} \left(t - \frac{T_{\text{ch}}}{2} - \tau_{\text{cl}} \right) \right] e^{i\{kx - \omega_0 [t - (T_{\text{ch}}/2)]\}}. \end{aligned} \quad (39)$$

The conditions above make it possible to expand the multiplication factor and the argument of the first sine function in Eq. (34) around the classical time up to zeroth order, as well as to keep only the linear term in the argument of the second sine function and the phase. That way solution (39) is a product between the solution for stationary single-slit diffraction and the solution for diffraction at the slit in time. These solutions have the same analytic form of spatial y dependence and of time dependence, respectively, when converting quantities $a \leftrightarrow T_{\text{ch}}$, $k_0 \leftrightarrow \omega_0$, $x \leftrightarrow \tau_{\text{cl}}$, and $y \leftrightarrow t - \tau_{\text{cl}}$. Thus there is an analytical equivalence between the y dependence of the diffraction pattern in space for a fixed time and fixed x coordinate [Fig. 12(a)] on the one hand and the diffraction pattern in time for a fixed space point [Fig. 12(b)] on the other hand. Actually the expansion of solution (34) around the classical time removes the asymmetry between the space and time dependencies of the diffraction pattern which arises due to the different roles of space and time in the Green's function (9) for the Schrödinger wave. Solution (39) corresponds to the solution obtained in Refs. [4] and [5] by the stationary phase method. It is not surprising that conditions (38) are not satisfied in our example. Yet, with a wider slit ($a = 10^{-6}$ m) and a longer chop time ($T_{\text{ch}} = 10^{-6}$ s) they become satisfied.

C. Double slit in space and single slit in time

Now we assume that the screen contains two slits of equal width a which are opened simultaneously at $t = 0$ and closed again at $t = T_{\text{ch}}$. Let the inside edges of the slits be placed at $y = -b/2$ and $b/2$. Then, by translation of expression (26) along the y axis, we immediately obtain the solution of the present problem:

$$\psi(x, y, t) = \psi^{\text{slit}}\left(x, y - \frac{b}{2} - \frac{a}{2}, t\right) + \psi^{\text{slit}}\left(x, y + \frac{b}{2} + \frac{a}{2}, t\right),$$

where $\psi^{\text{slit}}(x, y, t)$ is taken from Eq. (26). Figure 13 shows the resulting wave packet for our Li-atom example with $b = 2 \times 10^{-7}$ m.

Now we shall first obtain positions of the interference minima in space and in time neglecting the finite dimensions of the slits and the finite chop time. The solution is then a superposition of the secondary waves coming from point sources. The phases of the secondary waves are

$$\phi_1(x, y, t) = \frac{m\{x^2 + [y + (b/2) + (a/2)]^2\}}{2\hbar t}$$

and

$$\phi_2(x, y, t) = \frac{m\{x^2 + [y - (b/2) - (a/2)]^2\}}{2\hbar t},$$

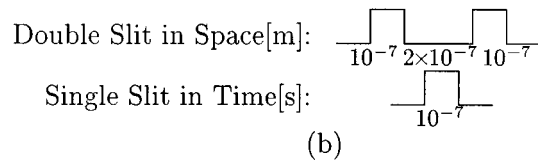
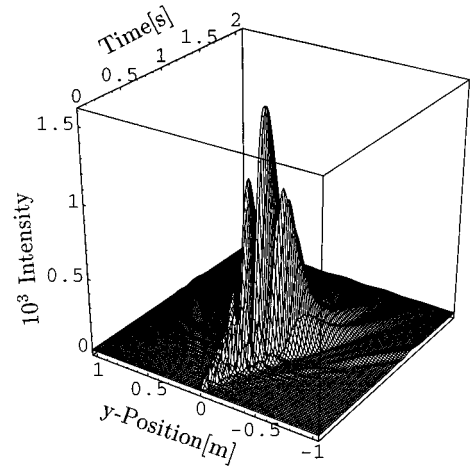
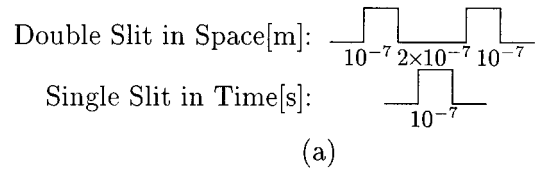
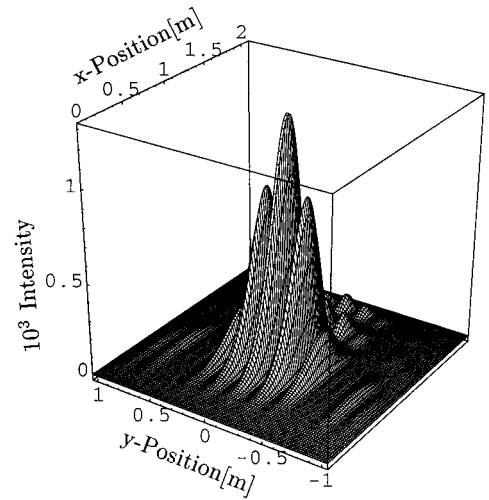


FIG. 13. Diffraction of Li-7 atoms with velocity $v_0 = 1$ m/s at a double slit in space and a single slit in time. The atoms are again incident along the positive- x direction onto the double slit located at $x = 0$ and $y = 0$ which opens for 10^{-7} s at $t = 0$. The individual slits are each 10^{-7} m wide and they are separated by 2×10^{-7} m. The parameters are chosen such that both diffraction in time and diffraction in space are very pronounced. The well-known Young's fringes are clearly visible. The top (a) is again a picture of the wave packet at $t = 1$ s, and below (b) we see the arrival times at the observation screen $x = 1$ m.

respectively [see the Green's function (9)]. These values correspond to the phase factors of the two packets given above in the Fraunhofer limit in space and in time, see Eq. (34), and are therefore also applicable to our Li-atom example.

For those points in space and in time where the phase difference between the two waves is an odd multiple of π ,

$$\phi_1(\mathbf{r}_{\min}, t_{\min}) - \phi_2(\mathbf{r}_{\min}, t_{\min}) = (2n+1)\pi, \quad (40)$$

we find positions of interference minima in space and in time

$$y_{\min} = \frac{(2n+1)h[t - (T_{\text{ch}}/2)]}{2m(a+b)}, \quad n \in \mathbb{Z}. \quad (41)$$

The lines of the interference minima parallel to the x axis for a certain observation time and their linear spreading in the course of time are seen in Figs. 13(a) and 13(b), respectively. The angular separation between the two first minima within the Fraunhofer approximation in space and in time is time independent, and equal to the one in the stationary case:

$$\Delta\alpha \equiv 2 \frac{y_{1,\min}(t)}{v_0 t} = 2 \frac{\lambda}{a+b}. \quad (42)$$

D. Single slit in space and double slit in time

Let a single slit be opened at $t=0$, closed at $t=T_{\text{ch}}$, and then again be opened at $t=T_{\text{ch}}+T_{\text{pause}}$ and closed at $t=2T_{\text{ch}}+T_{\text{pause}}$. Assuming that the initial wave in the left half-space is not influenced by the chopping, the boundary condition chosen can also be applied to the second chopped wave. Changing the integration area in the Eq. (26), one may then obtain the solution

$$\begin{aligned} \psi(x, y, t) = & \psi^{\text{slit}}(x, y, t) + e^{-i\omega_0(T_{\text{ch}}+T_{\text{pause}})} \\ & \times \psi^{\text{slit}}(x, y, t - T_{\text{ch}} - T_{\text{pause}}), \end{aligned} \quad (43)$$

where $\psi^{\text{slit}}(x, y, t)$ is taken from Eq. (26). This solution therefore is not just the sum of solution (26) and its translation in time (by $-T_{\text{pause}} - T_{\text{ch}}$). The resulting intensity distributions are given in Fig. 14 for our Li-atom example with $T_{\text{pause}} = 2 \times 10^{-7}$ s.

We now again discuss the positions of the minima. Neglecting again the finite dimensions of the slit and the finiteness of the chop times, we consider the two successive chopped waves as coming from point sources in space and in time. The phases of the secondary waves are $\phi_3(x, y, t) = m(x^2 + y^2)/2\hbar t$ and $\phi_4(x, y, t) = m(x^2 + y^2)/2\hbar(t - T_{\text{ch}} - T_{\text{pause}})$, respectively. From condition (40) we obtain the positions of the interference minima as

$$\begin{aligned} x_{\min}^2 + y_{\min}^2 = & v_0 \left(t - \frac{T_{\text{ch}}}{2} \right) \\ & - \frac{(2n+1)h[t - (T_{\text{ch}}/2)](t - \frac{3}{2}T_{\text{ch}} - T_{\text{pause}})}{2m(T_{\text{ch}} + T_{\text{pause}})}, \end{aligned} \quad (44)$$

$$n \in \mathbb{Z}.$$

Circles of the interference minima in space for a certain observation time and the corresponding hyperbolas of the interference minima in the y - t plane for a certain plane of observation are seen in Figs. 14(a) and 14(b) respectively.

Using a time-modulated light wave as an atomic mirror to

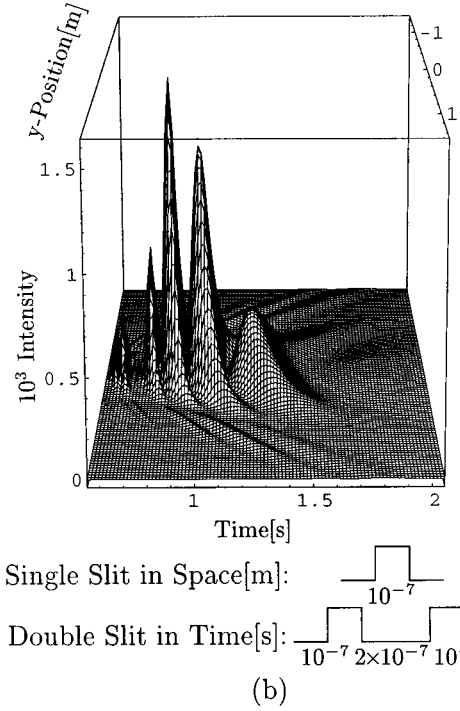
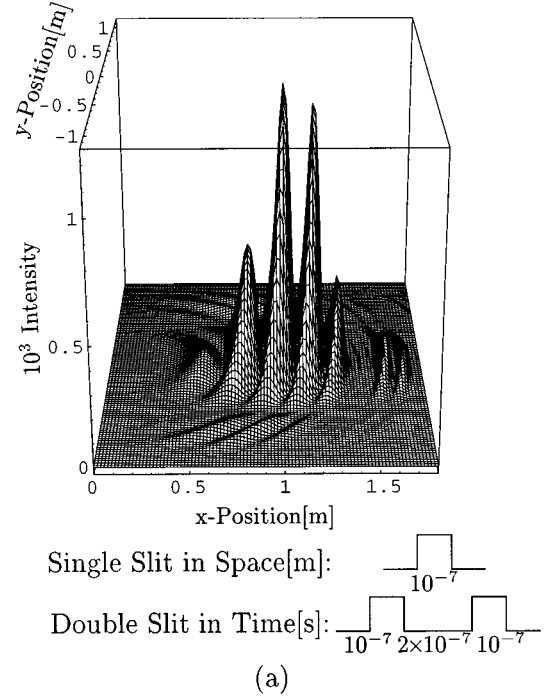


FIG. 14. A single slit in space and a double slit in time. Again, Li-7 atoms are incident along the positive x direction onto a single slit located at $x=0$ and $y=0$. The slit is opened successively twice, which results in the double slit in time. In the picture of the wave packet at $t=1$ s (a), one clearly sees that the double slit in time phenomenon exhibits the same characteristic Young's interference fringes well known for a double slit in space. This is confirmed by the picture of the arrival times (b).

chop a slow cesium atomic beam, Szriftgiser *et al.* [13] performed an experiment on the diffraction at temporal single and double slits, and measured the energy distribution of the chopped atoms.

E. Double slit in space and in time

This case is a combination of the previous two cases. Two slits of equal width a and of distance b between their inside edges are opened at $t=0$, closed at $t=T_{\text{ch}}$, and then again opened at $t=T_{\text{ch}}+T_{\text{pause}}$ and closed at $t=2T_{\text{ch}}+T_{\text{pause}}$. It is easy to construct the present solution from the last two cases:

$$\begin{aligned} \psi(x,y,t) = & \psi^{\text{slit}}\left(x,y-\frac{a}{2}-\frac{b}{2},t\right) + \psi^{\text{slit}}\left(x,y+\frac{a}{2}+\frac{b}{2},t\right) \\ & + e^{-i\omega_0(T_{\text{ch}}+T_{\text{pause}})} \left[\psi^{\text{slit}}\left(x,y-\frac{a}{2}-\frac{b}{2},t \right. \right. \\ & \left. \left. - T_{\text{ch}} - T_{\text{pause}}\right) + \psi^{\text{slit}}\left(x,y+\frac{a}{2}+\frac{b}{2},t \right. \right. \\ & \left. \left. - T_{\text{ch}} - T_{\text{pause}}\right) \right], \end{aligned} \quad (45)$$

where $\psi^{\text{slit}}(x,y,t)$ is taken from Eq. (26). Figure 15 demonstrates the wave packet for our Li-atom example with b and T_{pause} the same as in the previous two cases.

Neglecting again the finite dimensions of the slits and the finiteness of the chop times, we consider the four waves on the right-hand side of Eq. (45) as coming from point sources in space and in time in order to obtain an estimate for the minima. Omitting the amplitudes we write $\psi(x,y,t) \propto e^{i\phi_1(x,y,t)} + e^{i\phi_2(x,y,t)} + e^{i\phi_3(x,y,t)} + e^{i\phi_4(x,y,t)}$ with phases given in Secs. IV B and IV C. It is important to notice that $\phi_1(x,y,t) - \phi_2(x,y,t) \approx \phi_3(x,y,t) - \phi_4(x,y,t)$ for $T_{\text{ch}} + T_{\text{pause}} \ll t$ and $a+b \ll y$. This expression together with the condition $|\psi(x_m, y_m, t_m)|^2 = 0$ leads to the condition

$$\begin{aligned} & \cos[\phi_1(x_m, y_m, t_m) - \phi_2(x_m, y_m, t_m)] + \cos[\phi_1(x_m, y_m, t_m) \\ & - \phi_3(x_m, y_m, t_m)] + \cos[\phi_1(x_m, y_m, t_m) - \phi_2(x_m, y_m, t_m)] \\ & \times \cos[\phi_1(x_m, y_m, t_m) - \phi_3(x_m, y_m, t_m)] = -1. \end{aligned}$$

This is obviously satisfied when $\phi_1(x_m, y_m, t_m) - \phi_2(x_m, y_m, t_m) = (2n+1)\pi$ or/and $\phi_1(x_m, y_m, t_m) - \phi_3(x_m, y_m, t_m) = (2n+1)\pi$, where $n \in \mathbb{Z}$. Therefore, the present pattern exhibits both the interference minima which are present in the case of a double slit in space and a single slit in time, as well as those of the case of a single slit in space and a double slit in time and no other interference minima.

V. LIMIT FOR LARGE TIMES

Usually the accuracy of theoretical predictions decreases with increasing time. However, for some problems it is still possible to find not only exact solutions but also some general statements about the evolution of the system in the limit of large times. In this section we find the connection through Fourier transformation between an incident wave and the resulting time-modulated one in the limit of large times. In the theory of stationary diffraction it is well known that the patterns in the Fraunhofer limit represent the square of the Fourier transform in space of the incident wave in the aperture

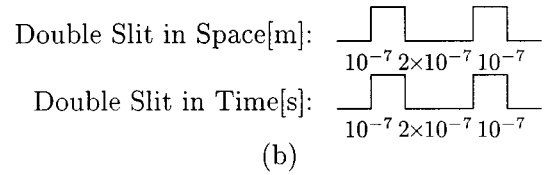
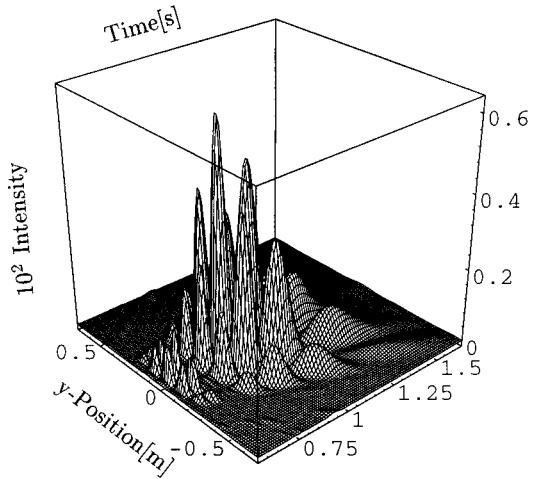
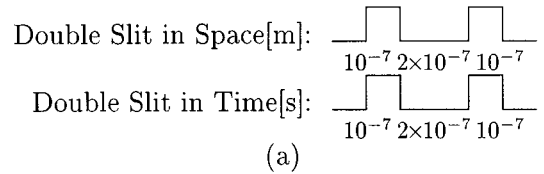
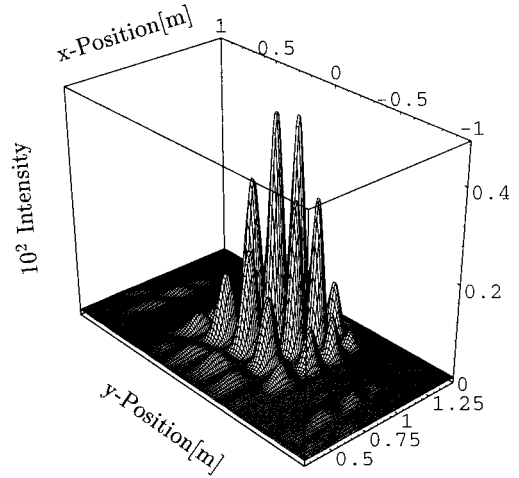


FIG. 15. Diffraction at a double slit both in space and time. Li-7 atoms are incident along the positive- x direction onto a double slit located at $x=0$ and $y=0$. This spatial double slit is opened twice successively such that a double slit in time also results. It is evident from the picture (a) of the wave packet at $t=1$ s that a number of different interference maxima and minima result, indicative of Young's fringes both in space and in time. This is confirmed by the time of arrival of the atoms in the observation plane located at $x=1$ m (b).

[14]. We now raise the question of whether the nonstationary diffraction patterns of matter waves in space and in time represent the square of a Fourier transform in space and in time of the incident wave in the time-dependent aperture.

This indeed turns out to be the case but only in a region around the classical time.

We shall discuss the long-time dynamics of an arbitrary wave incident onto a nontransmitting screen with a time-dependent aperture. The screen is again located at $x=0$. We assume that both the width of the aperture and the duration of the chopping are bounded in space and in time, respectively. Keeping the dimensions of the aperture finite, our problem becomes three dimensional. The boundary conditions can be summarized into a single complex function

$$\psi^a(y, z, t) = \begin{cases} \psi(0, y, z, t), & |y| < Y, \quad |z| < Z, \quad 0 \leq t \leq \tau \\ 0 & \text{otherwise,} \end{cases}$$

which we call the aperture function analogous to the quantity in stationary diffraction [14]. The function $\psi(0, y, z, t)$ is arbitrary. Because the aperture function is nonzero only within the bounds X , Y , and τ of spatial and temporal extensions of the aperture, respectively, the limits in integral (11) can be extended to $\pm\infty$,

$$\begin{aligned} \psi(\mathbf{r}, t) &= -\frac{ixm}{2\pi\hbar} \left(\frac{m}{2\pi i\hbar} \right)^{1/2} \int_{-\infty}^{+\infty} dt_0 \frac{1}{(t-t_0)^{5/2}} \\ &\times \int_{-\infty}^{+\infty} dy_0 \int_{-\infty}^{+\infty} dz_0 \psi^a(y_0, z_0, t_0) \\ &\times e^{im(x^2+y^2+z^2)/2\hbar(t-t_0)} e^{-imy_0/\hbar(t-t_0)} \\ &\times e^{imy_0^2/2\hbar(t-t_0)} e^{imz_0^2/2\hbar(t-t_0)}. \end{aligned} \quad (46)$$

It should be noted that all requirements considered in Sec. IV for the Fraunhofer limit in space and in time become satisfied when a sufficiently large time elapses. Therefore, the assumptions for the limit of large times considered here will only be generalizations of the ones used in the special case considered in Sec. IV. Thus, with the assumptions

$$\frac{mY^2}{2\hbar(t-\tau)} \rightarrow 0 \quad \text{and} \quad \frac{mZ^2}{2\hbar(t-\tau)} \rightarrow 0, \quad (47)$$

the fourth and fifth exponential integrands tend to 1. With the further approximations

$$\frac{m(x^2+y^2+z^2)\tau^2}{2\hbar t^3} \rightarrow 0, \quad \frac{myY\tau}{\hbar t^2} \rightarrow 0, \quad \frac{mzZ\tau}{\hbar t^2} \rightarrow 0, \quad (48)$$

the function $1/(t-t_0)$ in the arguments of the first, second, and third exponential integrands in Eq. (46) can be expanded around $t_0=0$ up to the zeroth-order term for the first exponential integrand and up to the linear terms for the other two exponential integrands. We treat the function $1/(t-t_0)^{5/2}$ to be a constant compared with other rapidly varying integrands. Thus we obtain

$$\begin{aligned} \psi(\mathbf{r}, t) &= \frac{xm^{3/2}}{t^{5/2}} e^{i(3\pi/4)} e^{im(x^2+y^2+z^2)/2\hbar t} \frac{1}{(2\pi\hbar)^{3/2}} \\ &\times \int_{-\infty}^{+\infty} dt_0 \int_{-\infty}^{+\infty} dy_0 \int_{-\infty}^{+\infty} dz_0 \psi^a(y_0, z_0, t_0) \\ &\times e^{im(x^2+y^2+z^2)/2\hbar t^2} t_0 e^{-i(my/\hbar t)y_0} e^{-i(mz/\hbar t)z_0}. \end{aligned} \quad (49)$$

Let us define the spatial frequencies k_y and k_z and the temporal frequency ω as

$$k_y = \frac{my}{\hbar t}, \quad k_z = \frac{mz}{\hbar t} \quad \text{and} \quad \omega = \frac{m(x^2+y^2+z^2)}{2\hbar t^2},$$

respectively. For each observation point in space and in time, there are corresponding spatial and temporal frequencies. Solution (49) can now be written as

$$\psi(\mathbf{r}, t) = \frac{xm^{3/2}}{t^{5/2}} e^{i(3\pi/4)} e^{im(x^2+y^2+z^2)/2\hbar t} \Phi(k_y, k_z, \omega), \quad (50)$$

where $\Phi(k_y, k_z, \omega)$ is the Fourier transform of the aperture function both in space, for y and z coordinates, and in time.

The asymptotic expansion (50) is in agreement with our expectation, since the larger the observation time t is, the smaller the contributing spatial and temporal frequencies of the aperture function are. Expression (50) is also in agreement with the Fraunhofer limit in space and in time (34) of the chopped semi-infinite monochromatic wave (Sec. IV). Thus the Fourier transform $\Phi(k_y, \omega)$ of the product of a rectangular function in space with a modulated rectangular function in time $(\theta[(a/2)-y] - \theta[(-a/2)-y])(\theta[t] - \theta[t - T_{\text{ch}}])e^{-i\omega_0 t}$ is

$$\Phi(k_y, \omega) = \frac{\sin(k_y a/2)}{k_y/2} \frac{\sin[(\omega - \omega_0)T_{\text{ch}}/2]}{(\omega - \omega_0)/2},$$

which, using Eq. (50) and taking into account the dimensionality of the problem, gives Eq. (34).

Since the space coordinates are not only involved in the spatial frequencies but also in the temporal frequency, the statement valid in stationary optics that the space dependence of patterns in the Fraunhofer limit represents the square of the Fourier transform in space of the incident wave in the aperture is no longer valid here in the nonstationary case. While the space dependence of the stationary pattern is completely determined by the Fourier transform in space of the incident wave, the space dependence of the nonstationary pattern is also influenced by its Fourier transform in time. This is most easily seen from Figs. 9–15, where the y dependencies of the diffraction patterns are not only influenced by lines of minima (35), corresponding to the minima in stationary diffraction which are related to the Fourier transform in space of the incident wave, but also by the circles of minima (36) related to its Fourier transform in time.

Now we shall examine the conditions for the validity of the statement above in nonstationary optics. Assuming that the particle speed after chopping $k_0\hbar/m$ is well defined (for a chop duration much longer than the de Broglie wave period of the incident wave) we expand the solution (50) around the classical time $\tau_{\text{cl}} \equiv m\sqrt{x^2+y^2+z^2}/k_0\hbar$. If, additionally, the spatial bounds X and Y are large compared to the wavelength, the mean width of the packet both along the y direction and along the z direction remains smaller than the distance reached along the x direction, and the classical time becomes $\tau_{\text{cl}} \approx mx/k_0\hbar$. Thus with the approximations

$$\frac{m(x^2+y^2+z^2)}{2\hbar\tau_{cl}} \left(\frac{t-\tau_{cl}}{\tau_{cl}} \right)^2 \rightarrow 0, \quad \frac{myY}{2\hbar\tau_{cl}} \frac{t-\tau_{cl}}{\tau_{cl}} \rightarrow 0,$$

$$\frac{mzZ}{2\hbar\tau_{cl}} \frac{t-\tau_{cl}}{\tau_{cl}} \rightarrow 0 \quad \text{and} \quad \frac{3m(x^2+y^2+z^2)}{2\hbar\tau_{cl}^2} \left(\frac{t-\tau_{cl}}{\tau_{cl}} \right)^2 \rightarrow 0, \quad (51)$$

the phase in Eq. (50) can be expanded retaining the first-order term as well as the arguments of the Fourier transform $my/\hbar t$ and $mz/\hbar t$ up to zeroth order and $m(x^2+y^2+z^2)/2\hbar t^2$ up to first order. That way the spatial frequencies no longer depend on time, and the temporal frequency no longer depends on space:

$$\psi(\mathbf{r}, t) \propto x e^{i(k_0 x - \omega_0 t)} \Phi(k_y, k_z, \omega), \quad (52)$$

where now $k_y = k_0 y/x$, $k_z = k_0 z/x$, $\omega = [2\omega_0(t - \tau_{cl})/\tau_{cl}] + \omega_0$. Equation (52) tells us that for a fixed x coordinate in the region around the classical time, the space dependence (y and z dependences) and the time dependence of the diffraction pattern represent the dependence on the spatial frequencies (k_y and k_z) and on the temporal frequency (ω) of the square of the Fourier transform in space and in time, respectively, of the incident wave in the time-dependent aperture. Obviously, this result is significant for the evolution of ‘‘nearly classical’’ wave packets.

VI. CONCLUDING COMMENTS

The Green’s function of the Schrödinger equation together with initial and boundary conditions contains all quantum mechanically allowed information about the system considered. Seen as an effect of a point source in space and in time, the Green’s function enriches our understanding and helps us to solve nonstationary diffraction problems.

Huygens’s principle, postulating that each point on the wave front acts as a point source of secondary waves, supplemented by Fresnel with the statement that these secondary waves are mutually coherent, is basic for the Fresnel method of an intuitive description of stationary diffraction. The solution, involving some time-dependent boundary conditions, is equivalent to that of an appropriate time-dependent distribution of sources over the boundary surface, thus extending Huygens’ and Fresnel principles to nonstationary problems. This leads to the introduction of Fresnel zones in time by appropriately dividing the time axis of emission of the secondary waves. The center of the zeroth zone is determined by the time emission of the classical particle. The graphic addition of the amplitudes of secondary waves leads to a spiral, analogous to the well-known Cornu spiral of stationary diffraction. With the help of the concept of Fresnel zones in time, we introduced a device which we call the temporal Fresnel lens.

In the present calculations we used a boundary condition approach. We assumed Dirichlet conditions and found equivalent counterparts in initial conditions.

In the physics of electromagnetic waves in vacuum, the solution for an ‘‘edge in time’’ has a sharp shadow in time, while for matter waves it has a close resemblance to the

solution for stationary diffraction at an edge in space. Thus, in analogy to stationary diffraction at an edge in space, the transitional region from ‘‘time shadow’’ to ‘‘time-illuminated region’’ for the diffraction at the edge in time is of the order of $\sqrt{T\tau_{cl}}$, where T is the de Broglie wave period and $\tau_{cl} \equiv mx/k_0\hbar$ is the time a classical particle needs to travel from 0 to x . The classical limit of the solution for matter wave diffraction at the edge in time is equivalent to the solution for diffraction at the edge in time for electromagnetic waves.

We also calculated the time-dependent wave function resulting from the passage of a semi-infinite monochromatic beam through a slit with time varying width. Such two-dimensional problems imply simultaneous diffraction in space and in time. We computed and analyzed in detail the analytical solutions for various slit opening functions: edges in space and in time, single slits in space and in time, a double slit in space and a single slit in time, a single slit in space and a double slit in time, as well as double slits in space and in time. Due to the different roles of space and time for Schrödinger Green’s function, diffraction patterns in space and in time do not have fully equivalent space and time dependencies.

A wave diffracted at the edge in space and in time is a superposition of the freely propagating incident wave (present only in the illuminated region) and the one scattered from the edge (present both in the illuminated region and in the geometric shadow). The solution in the light-shadow boundary exhibits transitional regions both in space of the order $\sqrt{\lambda x}$ (λ is the de Broglie wavelength) and in time of the order $\sqrt{T\tau_{cl}}$. Only within the geometric shadow and around the light-shadow boundary is the solution for the diffraction at the edge in space and in time the product of the solution for stationary diffraction at an edge in space and the solution for diffraction at the edge in time.

In the Fraunhofer limit the solution for diffraction at the slit both in space and in time is a product of two terms closely associated with both the position-momentum and time-energy uncertainty relations. Our results are still valid when the conditions for simultaneous strong diffraction in space and in time are satisfied, that is, when the slit width a becomes comparable with the de Broglie wavelength λ , and the chop time T_{ch} becomes comparable with the de Broglie wave period T . The different space and time dependencies of the diffraction pattern become equivalent only for times in the region around the classical propagation time τ_{cl} . Such expansion of the solution around the classical time only makes sense for the evolution of ‘‘nearly classical’’ wave packets when the chop times are much longer than the de Broglie wave period and the slit widths are much larger than the de Broglie wavelength. Then the solution becomes a product between the solution for stationary diffraction at the slit in space and the solution for temporal diffraction at the slit in time.

Combining a double slit in space with a single slit in time as well as a single slit in space with a double slit in time, we obtain solutions exhibiting Young’s interference fringes in space and time, respectively. For diffraction at a double slit both in space and in time we find a highly structured packet with simultaneous Young’s fringes in space and in time.

Through Fourier transformation we found a connection

between an incident wave and a resulting time-modulated wave in the limit of large times. It is shown that in the region around the classical time, diffraction patterns in space and in time can be represented as the square of the Fourier transform both in space and in time of the incident wave in the time-dependent aperture. This is a generalization of the well-known analogous situation in stationary diffraction.

We regard our calculations as a further step toward successfully preparing precision de Broglie wave diffraction ex-

periments for atoms, molecules, and possibly heavier objects.

ACKNOWLEDGMENTS

This work was supported by the Austrian Fonds zur Förderung der wissenschaftlichen Forschung Project No. S56504 and by the National Science Foundation under Grant No. PHY97-22614.

-
- [1] M. Born and E. Wolf, *Principles of Optics* (Pergamon, Oxford, 1980), pp. 387–392.
 - [2] A. Lagendijk and B. A. van Tiggelen, *Phys. Rep.* **270**, 143 (1996).
 - [3] M. Moshinsky, *Phys. Rev.* **88**, 625 (1952).
 - [4] R. Gaehler and R. Golub, *Z. Phys. B* **56**, 5 (1984).
 - [5] J. Felber, R. Gaehler, and R. Golub, *Physica B* **151**, 135 (1988).
 - [6] J. Kamesberger and A. Zeilinger, *Physica B* **151**, 193 (1988).
 - [7] J. Felber, G. Mueller, R. Gaehler, and R. Golub, *Physica B* **162**, 191 (1990).
 - [8] P. M. Morse and H. Feshbach, *Methods of Theoretical Physics* (McGraw-Hill, New York, 1953), pp. 791–895.
 - [9] H. M. Nussenzveig, *Causality and Dispersion Relation* (Academic, New York, 1972), pp. 59–76.
 - [10] Walter Gautschi, in *Handbook of Mathematical Functions*, edited by Milton Abramowitz and Irene A. Stegun (Dover, New York, 1970), p. 304.
 - [11] M. Arndt, P. Szriftgiser, J. Dalibard, and A. M. Steane, *Phys. Rev. A* **53**, 3369 (1996).
 - [12] W. Thirring, *Lehrbuch der Mathematische Physik—Klassische Feldtheorie* (Springer-Verlag, Vienna, 1990), p. 130.
 - [13] P. Szriftgiser, D. Guéry-Odelin, M. Arndt, and J. Dalibard, *Phys. Rev. Lett.* **77**, 4 (1996).
 - [14] See, e.g., E. Hecht, *Optics* (Addison-Wesley, Reading, MA, 1987), pp. 493–498.